SAPIENZA
UNIVERSITÀ DI ROMA

Molecular bases of Zimmermann-Laband syndrome

PhD school: Biology and Molecular Medicine

PhD course: Human Biology and Medical Genetics (XXIX cycle)

Curriculum: Medical Genetics

Candidate

Dr. Stefano Paolacci

Tutor

Dr. Viviana Caputo

A/A 2016/2017

Summary

Abstract

Zimmermann-Laband syndrome (ZLS; MIM135500) is a rare developmental disorder characterized by facial dysmorphism, including coarsening of the face, bulbous soft nose, gingival enlargement, nail aplasia or hypoplasia, hypertrichosis, and intellectual disability, with or without epilepsy. To date, about 40 patients have been described with features fitting ZLS.

With the aim of identifying ZLS causative gene/s a WES approach on three ZLS patients was performed and allowed us to identify two disease genes, *KCNH1* and *ATP6V1B2* (Kortum *et al*., 2015). An enlargement of the cohort was performed through the recruitment of further five patients, that were analyzed by WES or Sanger sequencing, disclosing the presence of additional mutations in *KCNH1* and *ATP6V1B2* genes (Kortum *et al*., 2015), and highlighting the role of potassium channels and vacuolar ATPase in the pathogenesis of this disease.

KCNH1 gene encodes a member of the potassium channel, voltage-gated, subfamily H protein. Patch-clamp recordings on KCNH1 mutants identified in this work showed strong negative shifts in voltage-dependent activation, supporting a possible gain-of-function effect for all ZLS-associated KCNH1 mutants.

ATP6V1B2 gene encodes the B2 subunit of the multimeric vacuolar H^+ ATPase. Structural analysis predicts a perturbing effect of the mutation on complex assembly.

Sanger sequencing screening of the coding sequence of the *KCNH1* and *ATP6V1B2* genes in four patients with clinical features within the ZLS clinical spectrum, disclosed the presence of mutation-negative patients, pointing to genetic heterogeneity for ZLS. To identify the "missing" ZLS disease genes, a WES approach on two *KCNH1* and *ATP6V1B2* mutation-negative subjects was performed, disclosing the presence of a novel likely pathogenic *de novo* variant in *ATP6V1C1*, encoding an interactor of ATP6V1B2.

Common clinical features of patients mutated in *KCNH1*, *ATP6V1B2* and *ATP6V1C1* genes include craniofacial dysmorphism, gingival enlargement, mild to severe intellectual disability, and aplastic or hypoplastic nails and terminal phalanges, although with remarkable variability. Epilepsy is present only in *KCNH1* mutated patients.

A recruitment of additional ZLS and ZLS-related patients is ongoing; these subjects will be screened for mutations in previously and newly identified disease genes in order to provide a more accurate picture of the molecular spectrum of mutations and their associated clinical spectrum.

Structural and functional studies are ongoing to characterize the effect of the ATP6V1B2 and ATP6V1C1 mutants on the proper assembly/activity of the ATPase complex.

1. Introduction

1.1 Zimmermann-Laband Syndrome: review of the literature

Zimmermann-Laband syndrome (ZLS; MIM135500), firstly described by Zimmermann (1928) in two patients, is a rare developmental disorder characterized by facial dysmorphism, such as coarsening of the face, bulbous soft nose, gingival enlargement and thick floppy ears, nail aplasia or hypoplasia, hypertrichosis, and intellectual disability, with or without epilepsy (Balasubramanian and Parker, 2010). Although, Zimmermann is considered the first describing this condition, a patient with similar features has been reported in 1886 by Humphry, which presented a patient with only the left side of the body affected. She showed gingival hyperplasia, long eyelashes and eyebrows, thick floppy ear, facial hypertrichosis, hypoplasia of nail and terminal phalange of the second digit of the foot (figure 1).

Figure 1. Original drawing of the patient described by Humphry (1886). Unilateral gingival hyperplasia can be observed.

Laband (1964) and Alavandar (1965) reported two Asiatic Indian families in which gingival fibromatosis occurred in association with hypoplasia of the terminal phalanges and absence or dysplasia of the fingernails. The report by Laband (1964) described the disorder in an East Indian 38-year-old woman and 5 of her 7 children. The mother showed large, soft ears, hypertension, hyperextensibility of metacarpophalangeal joints, and splenomegaly. The affected children had soft tissue enlargement of the nose and ears, splenomegaly, skeletal abnormalities, reduced size of toenails and thumbnails, short terminal phalanges, and hypermobility of several joints. The report by Alavandar (1965) described 5 affected persons in 3 generations with associated features of thickening of the soft tissues of the nose and ear with softness of the cartilages, hyperextensible joints, and hepatomegaly.

Chodirker *et al.* (1986) reported a case of a syndrome that he named for the first time Zimmermann-Laband, characterized by profound mental retardation, gingival fibromatosis, and absence of nails of thumbs and halluces.

Pina-Neto *et al.* (1988) reported a female patient with bulbous soft nose, thick floppy ears, gingival hypertrophy, large tongue, generalized hypertrichosis, joint laxity, hepatosplenomegaly, hypoplasia of distal phalanges of thumbs, thumbnails and toenails, generalized hypotonia, delayed neuromotor and speech development, mild mental retardation, lordosis, and flat feet.

Bakaeen and Scully (1991) described two siblings with Zimmermann-Laband syndrome, characterized by a pronounced gingival hyperplasia, thickened and enlarged ears and nose, nail dysplasia, hypoplastic terminal phalanges, hyperextensibility of the joints, and hepatosplenomegaly.

In 1992, Pfeiffer *et al.* described two patients with gingival fibromatosis, swelling of perioral tissues, nail hypo/aplasia, and abnormalities of terminal phalanges. 1 of the two patients suffers from epileptic seizures and shows osseous mandibular hypertrophy, two maxillary mesiodentes and lumbar spondylodysplasia. In the same year, Koch and collaborators reported on a 10-year-old girl with a diagnosis of Zimmermann-Laband syndrome, associated with an atypical retinitis pigmentosa.

Van Buggenhout *et al.* (1995) reported a 54 year-old male patient with Zimmermann-Laband syndrome, showing severe mental retardation, gingival hyperplasia, bulbous soft nose, thick floppy ears, full eyebrows, nails aplasia, hypoplastic distal phalanges with abnormal shape of the thumb phalanges of hands and feet, and scoliosis.

Robertson *et al.* (1998) reported on a 4-decade follow-up of a male with Zimmermann-Laband syndrome who developed a cardiomyopathy and dilatation of the aortic root and arch.

Dumic *et al.* (1999) reported a Croatian son of non consanguineous parents that had gingival hyperplasia and overgrowth of the major portion of the palatal tissue, bulbous soft nose and ears, hypoplastic toenails, hyperextensibility of the metacarpophalangeal joints, deep palmar and plantar crease, large tongue, and hypoplastic toenails.

In the report of a balanced reciprocal translocation in mother and daughter by Stefanova *et al.* (2003), the 40-year-old proposita had been referred to the dental clinic at age 16 years because of excessive gingival growth that completely covered the tooth crowns. She and her daughter, showed gingival hyperplasia, large fleshy nose, macrostomia, full lips, large tongue, large thick eyelashes, and normal intelligence. The mother showed dystrophic fingernails and aplasia of the toenails, whereas the daughter had aplasia of both the fingernails and toenails, prominent ears, and generalized hirsutism.

Shah and coworkers (2004) presented an unusual case of Zimmermann-Laband syndrome in a young male with bilateral developmental cataract.

In 2005, Holzhausen and collaborators published a report describing a 13-year-old female patient with previously undiagnosed Zimmermann-Laband syndrome, having the following clinical

and radiographic alterations: thick floppy ears, bulbous soft nose, prominent maxillae, thick lips, thick eyelashes and eyebrows, mild hirsutism, hypertelorism, telecanthus, short neck, high foot arch, hypoplasia of toenails, deformed terminal phalanges of the toes and thumbs, and hyperextensibility of the metacarpophalangeal joints, and supernumerary teeth. The patient did not have intellectual disability.

Davalos *et al.* (2005) reported two unrelated children, a boy and a girl, clinically and radiologically diagnosed with ZLS who displayed previously unreported features, such as: marked body overgrowth, cavernous hemangiomata in the frontal and left cerebellar regions in the boy, and unusual radiologic characteristics including broad medullary canals and metaphyses of the long bones, thin cortices, broad ribs, and accelerated skeletal maturation in the girl. The boy had psychomotor delay, whereas the girl had normal intelligence. The girl's mother and two brothers had also mild hypertrichosis but no other features of ZLS. The boy's father had soft tissue enlargement of the nose, ears, and lips.

A further 4-months-old male subject with ZLS was reported by Atabek *et al.* in 2005. He was the first child of a young non consanguineous couple. The upper part of his mouth showed a hyperplastic gingiva, and, in addition, he had a markedly generalized hypertrichosis, dysplastic nails of the fingers and toes, hyperpigmented scrotal skin, hyperextensible metacarpophalangeal joints, and deep palmar and plantar creases.

Hoogendijk and coworkers reported in 2006 a 14-year-old child with a gross hypertrophy of the maxillary and mandibular gingiva. His facial features include a bulbous soft nose, thick upper and lower lips, a low anterior hairline, and bushy eyebrows. Abnormalities of the nails of the feet were noted.

In the work of Kim *et al.* (2007), a male 46,XY,t(3;17)(p14.3;q24.3) with gingival hyperplasia, hypertrichosis, unusually large ears and marked hypertrophy of the nose is presented.

Abo-Dalo (2007 and 2008) reported three novel patients with ZLS. They shared as main clinical features hypoplastic terminal phalanges, aplastic nails, gingival fibromatosis, and mental retardation. One of them had macrocephaly and behavioral problems, another one had bulbous flat nose, macroglossia, hypertrichosis, while the third one had seizures, microcephaly, short stature, and scoliosis. Those three subjects were analyzed in the present research project, and correspond to case 5, 6 and 8, respectively.

Lin *et al.* described a patient with ZLS diagnosis in 2010. The diagnosis was made on the presence of gingival fibromatosis, bulbous nose, thick lips, hirsutism, deformed terminal phalanges, splenomegaly, and mental retardation. The patient exhibited also supernumerary teeth and thymic hyperplasia.

Chacon-Camacho and collaborators (2011) expanded the phenotypic spectrum of ZLS, reporting a patient with colpocephaly, hemivertebra, polydactyly, hyperpigmentation, and hemihyperplasia.

Davalos *et al.* (2011) reported a 9-year-old girl with Zimmermann-Laband syndrome. The patient had macrosomia, macrocephaly, generalized hypertrichosis, hepatomegaly, nail hypoplasia, gingival hyperplasia, and facial dysmorphism. She had severe bilateral sensorineural hearing loss. An additional patient was reported by Sawaki *et al.* (2012) having the classical features of ZLS.

Castori *et al.* (2013) described two unrelated subjects with Zimmermann-Laband syndrome who were analyzed in the current study (corresponding to case 1 and 2 in this work). One patient, was the unique son of unrelated parents. He had mild generalized hypertrichosis, anonychia of the thumbs and great toes, hypoplasia of nails of the fifth fingers and fourth left finger, gingival hypertrophy, soft nose, his psychomotor development was delayed with severe motor impairment, and seizures. The second patient, was a 5-year-old girl. She was the only child of two non consanguineous parents. At birth, she had generalized hypotonia, coarse face, hirsutism, and nails hypoplasia of hands and feet, aplasia or hypoplasia of phalanges on both hands and feet, delayed psychomotor development, gingival hypertrophy, soft nose and ear cartilages, and hirsutism. Figure 2 illustrates some pictures representing the most typical features of Zimmermann-Laband syndrome.

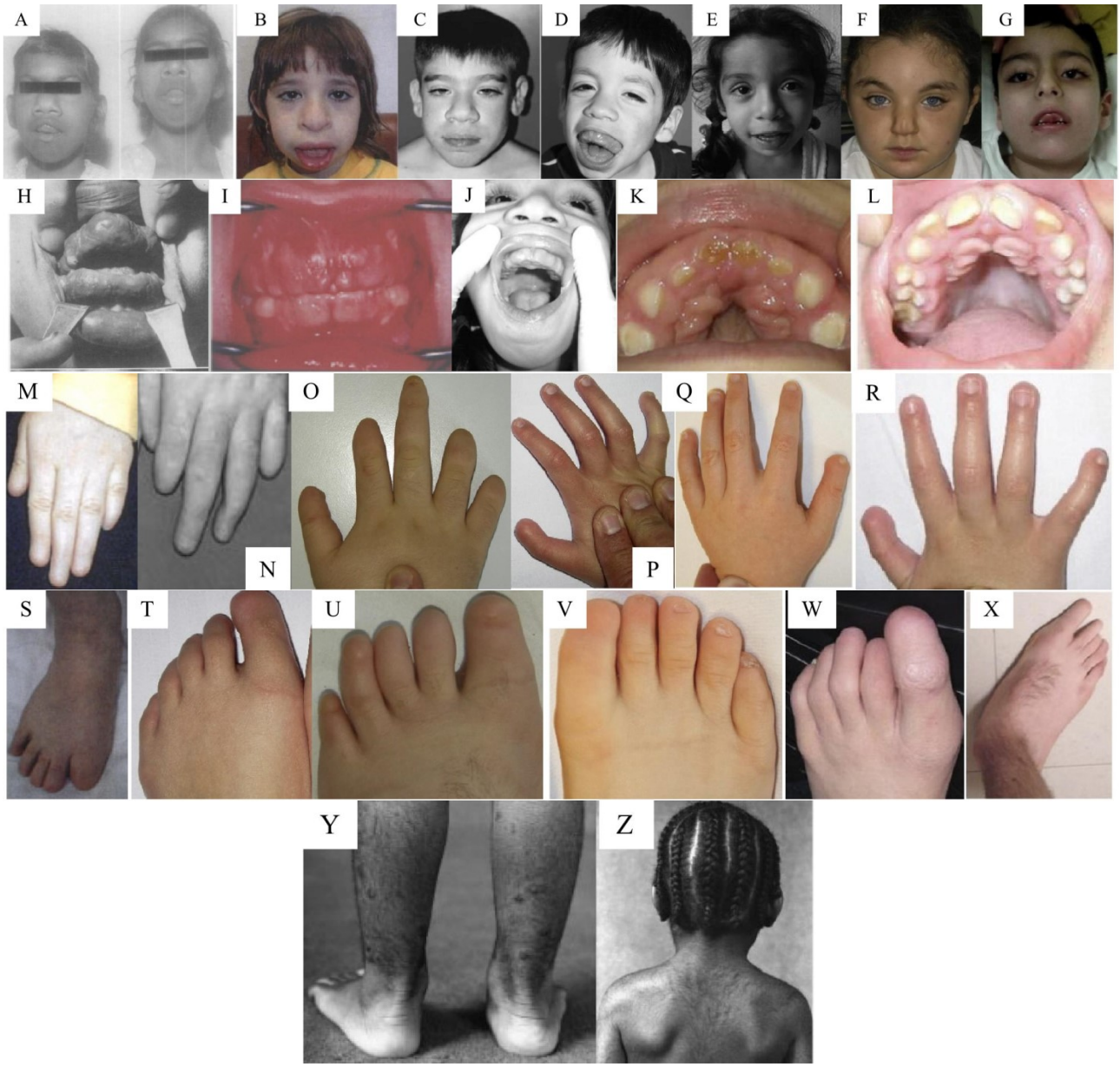

Figure 2. Main ZLS features. (A-G) Typical facial appearance of ZLS patients, with flat nasal bridge, bulbous nose, thick ears, in D gingival hyperplasia can be observed; (H-L) Picture showing gingival hyperplasia; (M-R) pictures showing aplasia/hypoplasia of nails and terminal phalanges of hands, in M, N, and O the aplasia of nails and hypoplasia of terminal phalanges is evident, in P, Q and R hypoplasia of nails; (S-X) pictures showing aplasia of feet nails, in S and X can also be noted hypertrichosis; (Y,Z) two pictures showing an example of back and limb hirsutism.
(A and H, Laband *et al.,* 1964; B, I, M and S, Stefanova *et al.,* 2003; C and N, Abo-Dalo *et al.,* 2008; D, Balasubramanian and Parker, 2010; E and J, Davalos *et al.,* 2011; F, K, O, P, T and U, Castori *et al.,* 2013; L, Q, R, V-X, Kortum *et al.,* 2015; Y and Z, Kim *et al.,* 2007)

1.2 Clinical features of Zimmermann-Laband syndrome

All the patients reported in literature with the diagnosis of ZLS share some clinical features, such as gingival hyperplasia, hypoplasia or aplasia of nails and phalanges. Most of them have bulbous soft nose and thick lips, and in different proportion: soft dysmorphic ears (40%), joint hypermobility (48%), generalized hypertrichosis (37%), intellectual disability (40%), and epilepsy

(14%). Other less frequent characteristics are: thick eyebrows and long eyelashes (27%), hypertelorism (12%), downslanting palpebral fissures (10%), micrognathia (27%), high-arched or cleft palate (21%), supranumerary teeth or hypodontia (12%), macroglossia (23%), joint contractures (4%), hypotonia (12%), *pes planus* or *cavus* (10%), *hallux valgus* (8%), short neck (10%), spine anomalies (15%), undertubulated long bones (4%), growth delay or short stature (8%), hemihyperplasia or body overgrowth (4%), soft skin (12%), hyperpigmentation (4%), deep palmar or plantar creases (4%), cataract (6%), deafness (4%), hepatomegaly (27%), splenomegaly (17%), heart defects (12%), and abnormal genitalia (6%) (Castori *et al*., 2013). Most of the symptoms manifest during infancy. In table 1 a list of the main features of ZLS as reported in the clinical synopsis of OMIM is reported. An autosomal dominant inheritance with *de novo* mutations is the proposed mode of inheritance for this disease, even though autosomal recessive inheritance could not be excluded. X-linked inheritance was less likely because there is no reported imbalance between the two sexes.

ZIMMERMANN-LABAND SYNDROME FEATURES (MIM135500)	
TYPE OF ANOMALIES	**DESCRIPTION**
Weight	Weight at birth >90th centile
Facial dysmorphism	Coarse facies
	Prominent mandible
	Broad nasal bridge
	Fleshy nose
	Thick lips
	Gingival fibromatosis/hyperplasia
	High-arched palate
	Long, lobulated, posteriorly rotated ears
Hair anomalies	Thick eyebrows
	Synophrys
	Hypertrichosis
Hearing anomalies	Hearing loss (rare)
Vision anomalies	Myopia
	Cataracts
Teeth anomalies	Delayed tooth eruption
Cardiovascular anomalies	Cardiomyopathy
	Patent ductus arteriosus
	Aortic root/arch dilatation
Liver/Spleen/Kidneys anomalies	Hepatosplenomegaly
	Extrahepatic biliary atresia (rare)
	Renal calculi (rare)
Spine anomalies	Scoliosis
	Spina bifida occulta
Hands and feet anomalies	Hyperextensible fingers
	Hypoplastic distal phalanges
	Hypoplastic nails
Skin anomalies	Dry, thick skin
Neurological anomalies	Hypotonia
	Seizures
	Intellectual disability

Table 1. Main clinical features of Zimmerman-Laband syndrome as reported in clinical synopsis of OMIM.

1.3 Zimmermann-Laband-related syndromes

ZLS belongs to a group of syndromes characterized by considerable clinical overlap, such as autosomal recessive deafness, onychodystrophy, osteodystrophy, mental retardation, seizures syndrome (DOORS; MIM220500), Cantu syndrome (CS; MIM239850), Temple-Baraitser syndrome (TMBTS; MIM611816), and dominant deafness-onychodystrophy syndrome (DDOD; MIM124480).

Overlapping characteristics among those syndromes are coarse facies, absence or hypoplasia of phalanges and nails, seizures, intellectual disability, and hypertrichosis. There are also some

clinical differences, e.g. the autosomal recessive deafness, onychodystrophy, osteodystrophy, mental retardation, seizures syndrome (DOORS) has a more severe phenotype involving the central nervous system, vision anomalies (blindness, optic atrophy or cataract), profound sensorineural deafness, cerebral atrophy with enlarged ventricles, and peripheral polyneuropathy.

In Cantu syndrome (CS), cardiovascular malformations like cardiomegaly, congenital hypertrophy of left ventricle, bicuspid aortic valve, and patent ductus arteriosus are much more frequent. In addition, skeletal abnormalities as widened ribs, osteoporosis, platyspondily, and widened metaphyses are more frequently observed.

The dominant deafness-onychodystrophy syndrome (DDOD) differs from ZLS mainly for the constant presence of sensorineural hearing loss. Finally, Temple-Baraitser syndrome (TMBTS) is characterized by a more severe central nervous system involvement than ZLS, with delayed psychomotor development, seizures, intellectual disability, and hypotonia. In ZLS, those neurologic findings are not always present, and can have very different degrees of severity, from mild to very severe. A comparison among ZLS and the above cited syndromes is presented in table 2.

CLINICAL FEATURES	ZLS	TMBTS	CS	DOORS	DDOD
Overgrowth at birth	+	-	+	-	-
Coarse facies	+	-	+	+	-
Hearing loss	+	-	-	-	+
Myopia and/or cataracts	+	-	-	+	-
Broad nasal bridge	+	+	+	+	-
Fleshy nose	+	-	-	-	-
Thick lips	+	+	+	+	-
Gingival fibromatosis and/or hyperplasia	+	-	+	-	-
Aortic root and/or arch dilatation	+	-	-	-	-
Hepatosplenomegaly	+	-	-	-	-
Scoliosis	+	-	-	-	-
Joint hypermobility	+	-	-	-	-
Hypoplastic nails and/or distal phalanges	+	+	-	+	+
Hypertrichosis	+	-	+	-	-
Hypotonia	+	+	-	+	-
Seizures	+	+	-	+	-
Intellectual disability	+	+	+	+	-

Table 2. Major clinical features of ZLS, compared with four related syndromes. + = present; - = absent; ZLS = Zimmermann-Laband syndrome; CS = Cantu Syndrome; DOORS = deafness, onychodystrophy, osteodystrophy, mental retardation, seizures syndrome; DDOD = dominant deafness-onychodystrophy syndrome.

1.4 Molecular bases of ZLS-related syndromes

Mutated genes causative of ZLS-related syndromes have been identified in the last five years, using next generation sequencing approach, mainly whole-exome sequencing.

The first ZLS-related syndrome for which the molecular bases were characterized is the Cantu syndrome, caused by *de novo* mutations in the *ABCC9* gene (Harakalova *et al.,* 2012; van Bon *et al.,* 2012). The protein encoded by this gene is a member of the superfamily of ATP-binding cassette (ABC) transporters. ABCC9 is a member of the MRP subfamily which is involved in multi-drug resistance, and is thought to form ATP-sensitive potassium channels in cardiac, skeletal, and vascular and non-vascular smooth muscle.

Afterwards, mutations in the *TBC1D24* gene, encoding a protein with a TBC domain, were found to be causative of the DOORS syndrome (Campeau *et al.,* 2014; Azaiez *et al.,* 2014). TBC domain containing proteins may serve as specific GTPase-activating proteins, the Rab (Ras-related proteins in brain) small GTPases which are involved in the regulation of membrane trafficking. This protein is apparently not functionally linked to the ABCC9 protein.

Lately, the DDOD syndrome was found to be caused by a *de novo* truncating mutation in the *ATP6V1B2* gene (Yuan *et al.,* 2014), encoding a component of vacuolar ATPase (V-ATPase), a multisubunit enzyme that mediates acidification of eukaryotic intracellular organelles. V-ATPase dependent organelle acidification is necessary for protein sorting, zymogen activation, receptor-mediated endocytosis, and synaptic vesicle proton gradient generation. *ATP6V1B2* is highly expressed in osteoclasts.

Finally, Simons and coworkers (2015) found that TMBTS is caused by mutations in *KCNH1.* This gene encodes a pore-forming (alpha) subunit of a voltage-gated non-inactivating delayed rectifier potassium channel, subfamily H. It is activated at the onset of myoblast differentiation, and is highly expressed in brain. Since *ABCC9* and *KCNH1* encode proteins that constitute potassium channels, TMBTS and CS appear to be determined by a dysregulation of the intracellular potassium omeostasis.

1.5 Aim of the work

The aim of this project was the identification of genes underlying Zimmermann-Laband syndrome. To this aim, we selected a panel of clinically well-characterized ZLS patients, to be analyzed through a Whole-Exome Sequencing approach (WES). Our understanding of the molecular events underlying this condition could provide new tools for diagnosis of this rare disorder, with direct impact on diagnosis, prognosis, counseling, and patient management.

2. Materials and methods

2.1 Subjects

In this study, we selected, in the first step of the work, 3 subjects with a phenotype fitting the ZLS clinical features. They were clinically assessed by clinical geneticists and neurologists, from the Department of Pediatrics and Infantile Neuropsychiatry, "Sapienza" University of Rome, Department of Molecular Medicine, "Sapienza" University of Rome - San Camillo-Forlanini Hospital (Rome), Bambino Gesù Children's Hospital (Rome), respectively. Case 1 and 2 were previously reported by Castori *et al.,* 2013.

After the first step of recruitment and analysis, 5 further patients were added to the cohort, thanks to an international collaboration with the following centres: University of Hamburg (Germany), Zentrum für Kinder-und Jugendmedizin of Oldenburg (Germany), Sydney Children's Hospital (Australia), University of New South Wales (Australia), Saveetha Medical College and Hospital (India), University of Montreal (Canada), Centre Hospitalier de la Haute-Saône (France), Royal Children's Hospital and University of Melbourne (Australia), University of Montreal (Canada).

In a third step, 4 further patients were enrolled in the study, from the Università Cattolica del Sacro Cuore (Rome), Bambino Gesù Children's Hospital (Rome), Federico II University (Naples), and Azienda Ospedaliero - Universitaria "Meyer" (Florence).

Informed consent for DNA storage and genetic analyses was obtained from the parents or legal guardians of all subjects. Genetic studies were approved by all the institutional review boards of the participating institutions. Permission to publish photographs was given for all subjects shown in this work.

2.2 Sequencing approach

In the first 3 selected subjects (case 1, 2 and 3), we used a Whole-Exome Sequencing approach (WES). In case 2 and 3 we sequenced the trio, in case 1 only the proband. In a second phase of this study the ZLS cohort was expanded with 5 further patients. In two of them (case 4 and 8, and the relative parents) a WES approach was performed, while, in the other three subjects (case 5, 6, and 7) a Sanger sequencing of the coding portion of the newly identified genes was used. Validations of candidate variants of cases 4 and 8, and Sanger screening of cases 5-7 was performed by researchers from the University of Hamburg (Germany). Finally, the more recently selected patients (cases 9-12) were firstly analyzed by Sanger sequencing of the coding portion of the newly identified genes (*KCNH1* and *ATP6V1B2*), and then two patients (cases 9 and 10) were analyzed

through WES of the probands and their parents. WES data analysis of case 10 is still ongoing (table 3).

Case	Sequencing approach	Trio/Singleton	Enrichment kit	NGS platform
1	WES	Singleton	NimbleGen SeqCap EZ v3.0 (Roche)	HiSeq 2000 (Illumina)
2	WES	Trio	NimbleGen SeqCap EZ v3.0 (Roche)	HiSeq 2000 (Illumina)
3	WES	Trio	SureSelect AllExonV4 (Agilent)	HiSeq 2000 (Illumina)
4	WES	Trio	TruSeq Exome Enrichment kit (Illumina)	HiSeq 2000 (Illumina)
5	Sanger	/	/	/
6	Sanger	/	/	/
7	Sanger	/	/	/
8	WES	Trio	TruSeq Exome Enrichment kit (Illumina)	HiSeq 2000 (Illumina)
9	WES	Trio	SureSelect Clinical Research Exome kit (Agilent)	NextSeq500 (Illumina)
10	WES	Trio	SureSelect Clinical Research Exome kit (Agilent)	NextSeq500 (Illumina)
11	Sanger	/	/	/
12	Sanger	/	/	/

Table 3. Schematic representation of the sequencing approach performed on our cohort. WES = Whole-Exome Sequencing.

2.3 Whole-exome sequencing of ZLS selected patients

Targeted enrichment and massively parallel sequencing were performed on genomic DNA of seven cases and the parents of six of them (cases 2, 3, 4, 8, 9, and 10). The DNA was extracted from circulating leukocytes using the Gentra Puregene Blood Kit (Qiagen). Enrichment of the whole-exome was performed using the NimbleGen SeqCap EZ Library v.3.0 (64 Mb) (Roche) for cases 1 and 2 (and her parents), the SureSelect AllExonV4 (51 M) (Agilent) for case 3 and her parents, the TruSeq Exome Enrichment kit (Illumina) for cases 4 and 8 and their respective parents, and the SureSelect Clinical Research Exome kit for case 9 and her parents. Each captured library was then loaded onto the HiSeq 2000 platform (Illumina) for cases from 1 to 8 and onto the NextSeq500 platform (Illumina) for cases 9 and 10. Raw image files were processed for base calling by the on-instrument software.

2.4 Whole-exome sequencing: data analysis and variant/gene annotation

Reads were aligned to the human reference genome (UCSC GRCh37/hg19) using the Burrows-Wheeler Aligner v.0.7.10 (Li and Durbin, 2009). PCR duplicates were removed using Picard's MarkDuplicates.

Single Nucleotide Variants (SNVs) and small indels were identified by means of the GATK HaplotypeCaller and UnifiedGenotyper algorithms (McKenna *et al.,* 2010): the former calls SNVs and indels simultaneously via local *de novo* assembly of haplotypes. Whenever the program encounters a region showing signs of variation, it discards the existing mapping information and completely reassembles the reads in that region. This allows the HaplotypeCaller to be more accurate for difficult regions, for example containing variants mapping close to each other. HaplotypeCaller identifies more accurately indels than UnifiedGenotyper. The latter uses a Bayesian genotype likelihood model to estimate simultaneously the most likely genotypes. The called variants were filtered applying the following quality filters: variants with quality >100, and quality-by-depth score >1.5 (the quality parameter normalized by the number of the reads) were retained; variants below these thresholds or resulting from four or more reads having ambiguous mapping (this number being greater than 10% of all aligned reads) were discarded. Only variants called by both algorithms were considered.

Since the disease is very rare it could be hypothesized that the causative mutation is not present or is annotated with a very low frequency in databases containing data of the DNA variants of the population. Therefore, variants were annotated using frequency data obtained from publicly available databases (dbSNP138 for cases 1-8 and dbSNP142 for cases 9 and 10, and ExAC) and an in-house database.

dbSNP is the acronym of Single Nucleotide Polymorphism database (https://www.ncbi.nlm.nih.gov/snp), a public-domain archive for a broad collection of simple genetic polymorphisms. This collection of polymorphisms includes single-base nucleotide substitutions, small deletions or insertions, retroposable element insertions and microsatellite repeat variations. ExAC (Exome Aggregation Consortium) (http://exac.broadinstitute.org/) contains DNA variants obtained from 60706 unrelated individuals sequenced as part of disease-specific and population genetic studies (Lek *et al*., 2016). Finally, the in-house database is composed of variants identified through WES approach in subjects affected by different developmental diseases, and their parents studied in our research group and collaborating groups. This database represented a useful tool to filter variants that represent high frequency polymorphisms and recurrent artifacts due to sequencing technology.

We set as a Minor Allele Frequency (MAF) threshold 0.1%, and retained only not annotated variants, variants of unknown frequency, and variants with MAF <0.1%. We retained also clinically associated variants according to ClinVar database. ClinVar is a freely accessible, public archive of reports of the relationships among human variations and phenotypes, with supporting evidence.

To predict the functional impact of variants, we used SnpEff toolbox v.3.6 (Cingolani *et al.,* 2013), an annotation tool that provides information at variant level: the effect of the variant on the transcript, the changed codon, and the isoform used to annotate the variant (usually the isoform for which the variant effect is greater or the longest isoform if the effect is the same).

Since the phenotype is very severe, it is likely that the causative variant(s) has(have) a great impact on the function of the protein or in the maturation of the transcript. We therefore retained only functionally relevant variants (i.e., missense, nonsense and coding indel variants and intronic variants located from −5 to +5 with respect to an exon-intron junction).

Further functional annotations regarding either the variant or the gene were added using SnpEff v.3.6 and dbNSFP v.2.5 (Cingolani *et al.,* 2013). Several scores were used to evaluate the functional impact of the variant on the function of the protein, e.g. Polyphen-2, SIFT, and CADD. Polyphen-2 predicts possible impact of an amino acid substitution on the structure and function of a human protein. This prediction is based on a number of features including the sequence, and phylogenetic and structural information related to the substitution. The substitution can be classified as “probably damaging”, “possibly damaging”, “benign” and “unknown”, if the lack of data does not allow to perform a prediction (Adzhubei *et al.,* 2010). SIFT (Sorting Tolerant From Intolerant) assesses the effect of a substitution assuming that crucial positions in protein sequences have been conserved throughout evolution and therefore substitutions at these positions may affect protein function. By using sequence homology, SIFT predicts the effects of all possible substitutions at each position in the protein sequence, with a score ranging from 0 to 1. The amino acid substitution is predicted as “damaging” if the score is <= 0.05, and “tolerated” if the score is > 0.05 (Kumar *et al.,* 2009). Combined Annotation-Dependent Depletion (CADD) is a tool for scoring the deleteriousness of single nucleotide variants as well as insertion/deletions variants in the human genome, integrating multiple annotations into one metric by comparing variants that survived natural selection with simulated mutations (Kircher *et al.,* 2014). It ranges from 0 to, theoretically, infinite, with a threshold of 15 usually used to consider a variant potentially pathogenetic.

Information regarding genes was retrieved from several databases such as: OMIM (Online Mendelian Inheritance in Man), a database that collects information about human mendelian diseases and/or phenotype and associated genes (https://omim.org/), Uniprot (Universal Protein Resource), a comprehensive resource for protein sequence and annotation data, used to obtain

information regarding the pathway in which the gene is involved (http://www.uniprot.org/), and GeneOntology (GO), a project that collects biological functions of genes at the molecular, cellular and tissue system levels (http://geneontology.org/).

2.5 Selection of candidate variants

After the steps of filtering and annotation of variants and genes, we selected the candidate variants using different criteria: segregation, effect of the variant, function of the gene, and involvement in a known disease.

Regarding the segregation, we considered different mode of inheritance: autosomal dominant, autosomal recessive, and X-linked. When possible, i.e. when the trio was sequenced, also the *de novo* variants were considered.

The variants were also prioritized considering the conservation of the amino acidic residue, pathogenicity/deleteriousness of the variant, and information about the function of the genes and their involvement in a known disease. As the three patients had the same clinical diagnosis, we looked at first for the presence of the same putative causative variant or different variants in the same gene in at least two patients.

2.6 Variant validation and mutation analysis

Candidate variants validation, segregation analyses, and Sanger screening were performed by PCR (GoTaq Flexi DNA Polymerase – Promega) followed by Sanger sequencing. Primers were designed in intronic regions flanking the coding exons of *KCNH1* (NC_000001.11, 210678315–211134115, complement), *ATP6V1B2* (NC_000008.11, 20197193-20221696), and *ATP6V1C1* (NC_000008.11, 103021020-103073057) in order to have the same annealing temperature. The amplification was performed using the following temperature cycle: initial denaturation at 95°C for 2', then the next three steps were repeated for 30 times, denaturation at 95°C for 30'', annealing at 60°C for 30'', elongation at 72°C for 30'', then final elongation at 72°C for 5', and finally the reaction was terminated at 4°C for 5'. Amplicons were directly sequenced using the ABI BigDye Terminator Sequencing kit (Life Technologies) and an automated capillary sequencer (ABI3500, Life Technologies). Sequence electropherograms were analyzed using Sequencing Analysis Software v.5.4 (Life Technologies). Genotyping was carried out with the AmpFlSTR Identifiler Plus (Life Technologies) to confirm paternity and maternity. The sequence of the primers used for amplification and sequencing are listed in the following tables (tables 4 and 5).

Gene	Name	Sequence (5'->3')	Gene	Name	Sequence (5'->3')
KCNH1	ex1_Fwd	gtttcctgctgtcgtaagaagc	***ATP6V1B2***	ex1_Fwd	cgttggcctgcacgcgtttg
	ex1_Rev	gaagagctctcctgttaggatg		ex1_Rev	cttctaaagagacaagtgggtc
	ex2_Fwd	tccttacagggcgacatttctg		ex2_Fwd	aagttgtataggcacagatgtag
	ex2_Rev	tcctgtgaatacacactaaatgag		ex2_Rev	gacacccagtctaaagtatggc
	ex3_Fwd	ttcttaatctaacttgagttctttg		ex3_Fwd	gagggtattgaaagctctcagc
	ex3_Rev	tcccaacatacacaagggcttc		ex3_Rev	atcggactaagtgacactgagc
	ex4_Fwd	tgtgataacccagcacttgaag		ex4+5_Fwd	ctgtaggcatgaacccttgatc
	ex4_Rev	ccttctcctaccccgatacac		ex4+5_Rev	ctatctggcaaaggtacaagac
	ex5_Fwd	agagtgactcatgggagcttag		ex6_Fwd	atgtagttctggtcttctggtg
	ex5_Rev	gattagcacactagttttgtgcc		ex6_Rev	gtgaggtaactggattatacaaac
	ex6_Fwd	ctcccatacttctttcatacctg		ex7_Fwd	ggtttcgtttatgattacgattcc
	ex6_Rev	atcaagcatgctccctctgttc		ex7_Rev	tgtacagcttactacaatgttctc
	ex7_Fwd	aagggttgcataaaattgcatctc		ex8_Fwd	gaaggaacaattcaaatctgtagc
	ex7_Rev	gctggcactgtagccatttcc		ex8_Rev	gttaggtccaaatgctgttattac
	ex8_Fwd	cctagtagcttggtggtaagag		ex9_Fwd	tcttttggtttgagtggcctaag
	ex8_Rev	gtaaggctgatctagaagcaaac		ex9_Rev	tctaatcacttctaccaagttgac
	ex9_Fwd	agagtgcagtctggcgtagtg		ex10_Fwd	tggcatgttgaaacaaacatgttg
	ex9_Rev	gaagcaatctctaactgaaggtg		ex10_Rev	tgttctcaaaataacttcaactcg
	ex10_Fwd	tttgccttctctgagcccaatc		ex11_Fwd	gtacagagggacttttgtggg
	ex10_Rev	tccatcttctaatctagcaacatc		ex11_Rev	agattcttaattctggcgctctg
	ex11_Fwd	cagccagcatgtggctaacac		ex12_Fwd	aggaagagacagtaggattcatc
	ex11_Rev	tgttggtcatgtggacatatgtg		ex12_Rev	atcttgatcatttgcatctgtcc
				ex13_Fwd	ctcttgtgaggagaactagagc
				ex13_Rev	gtgacagagcctcttctctaac
				ex14_Fwd	tggataacactgctaagttgg
				ex14_Rev	caacacaaaggtgggaaccg

Table 4. Sequences of the primers used to screen the coding sequences of *KCNH1* and *ATP6V1B2* genes.

Gene	Name	Sequence (5'->3')
ATP6V1C1	ex2_Fwd	cactttgcttgagatcctatgc
	ex2_Rev	taaatcatgccaatggctggag
	ex3_Fwd	tagggagaatttaagatttgtgag
	ex3_Rev	ccattccaataagcagagtatac
	ex4_Fwd	caaagtcttggtccattttatcc
	ex4_Rev	tgagattatgtttcagggaacag
	ex5_Fwd	atttcctcaatgccaatttcagc
	ex5_Rev	tctaagttgtaaggatttcttctg
	ex6_Fwd	aaatgacctcctaaagtcgtgc
	ex6_Rev	ccttagtgagcttttctccatg
	ex7_Fwd	actaagactaatccctctcaatg
	ex7_Rev	ttacgcttggattttatggaaaac
	ex8_Fwd	ttgaagtatacttactatagccag
	ex8_Rev	tcacaaaggcaagacagcaaac
	ex9+10_Fwd	tacttttctcttccacctgtttc
	ex9+10_Rev	aagctttagaggaaattcattctg
	ex11_Fwd	catgtagaaagtgaattatgcgac
	ex11_Rev	aagctgtatgatgatactgataatc
	ex12_Fwd	cgttaaccatgattaaagagtatg
	ex12_Rev	agggtaaacaatgtaaattactatg
	ex13_Fwd	agtgcatacatttagcccagag
	ex13_Rev	aagaagcaagcaaaggatactag

Table 5. Sequences of the primers used to screen the coding sequence of *ATP6V1C1* gene.

2.7 Haplotype determination

Case 1 carried two mutations in *KCNH1* gene, one in the exon 2 (inherited from the mother) and one in exon 7 (*de novo*). To evaluate the phase of the two variants, a fragment containing *KCNH1* coding sequence including exons from 2 to 7 was amplified, from cDNA obtained from the retrotranscription of total RNA extracted from patient cultured fibroblasts. Retrotranscription was performed using the SuperScript III Reverse Transcriptase (ThermoFisher), with random examers. The PCR product was cloned into the pCR2.1 TOPO TA Cloning Vector (Invitrogen), and the resulting plasmids were transformed into *E. coli*. Then, individual *E. coli* clones were picked and subjected to colony PCR and Sanger sequencing.

2.8 3D-Modeling

To preliminarily assess the effect of the mutations found in *KCNH1* and *ATP6V1B2*, 3D-modeling was performed in collaboration with researchers from the "Department of Sciences and Chemical Technologies", University of 'Tor Vergata' of Rome. Homology models of helices S5

and S6 of the K^+ voltage-gated channel, subfamily H member 1 (KCNH1) were generated, on the basis of the available crystallographic structures of homologous proteins, K_vAP voltage-dependent K^+ channel from *Aeropyrum pernix*, K^+ complex of the NaK channel, and the voltage-gated K^+ channel from *Listeria monocytogenes*.

Homology models of the B subunit (isoform 2) of the human V-ATPase (ATP6V1B2) were generated, on the basis of the ATPase from *Enterococcus hirae.*

2.9 Heterologous *KCNH1* expression in CHO cells and *Xenopus* oocytes

Electrophysiological experiments were performed in collaboration with researchers of the "Department of Cellular and Integrative Physiology", University Medical Center Hamburg-Eppendorf, of Hamburg (Germany), to test the effect of the mutations found in *KCNH1* gene. The used techniques are summarized in the following paragraphs.

cDNAs of wild-type or mutant human KCNH1 (hEAG1, isoform 1) and cDNA encoding EGFP-N1 (Clontech) were transfected in Chinese hamster ovary (CHO) cells using Lipofectamine 2000 (Invitrogen) (Schuster *et al.,* 2011).

cRNA encoding either wild-type KCNH1 channel or the KCNH1 mutant G469R were injected in *Xenopus* oocytes.

2.10 Electrophysiological studies

Patch-clamp experiments were performed 5–30h after CHO cell transfection or microinjection in the conventional whole-cell configuration of the patch-clamp technique. *Xenopus* oocyte currents were recorded with the two-electrode voltage-clamp technique. Patch-clamp data processing was performed with PulseFit 8.65 (HEKA), Excel (Microsoft) and Sigmaplot 11.0 (Systat Software). Current amplitudes were determined as mean values during the last period of the 2s test pulses or as maximal current amplitude for slightly inactivating current traces. Experimental data are given as means ± s.e.m., with *n* representing the number of experiments from different cells.

3. Results

3.1 Clinical features of selected ZLS subjects

Case 1 (figure 3) is an italian boy, the unique child of unrelated parents and was born at term (37 weeks) by vaginal delivery. Birth length was 47cm (3^{rd}-10^{th} centile), weight 2430g (3^{rd}-10^{th} centile) and occipital-frontal circumference of 33cm (3^{rd}-10^{th} centile). Additional findings at birth included absence of the first finger and toenails and mild generalized hypertrichosis. He stood up head at 10 months, walked alone at 24 months and said "mama" and "dada" at 12 months. Marked delay of the subsequent psychomotor development was noted with severe motor impairment, inability to communicate and lack of facial expressiveness. Seizures developed at 8 months of age in form of generalized stiffening episodes. Such a complication was treated by valproic acid and levetiracetam with partial remission of symptoms. At 2 years, brain MRI showed mild dilatation of the *cavum vergae*, and expansion of the subarachnoid spaces at the temporal lobes. Appendicular radiographic examination, performed at the same age, demonstrated hypoplasia of the 1^{st} distal phalanx at both hands and feet. Standard karyotyping and CGH array were negative. At 7 years, amino acid profile repeatedly revealed high plasmatic levels of hypoxanthine and xanthine. At examination, he weighted 21kg (25^{th}-50^{th} centile), was height 121cm (25^{th}-50^{th} centile) and had an OFC of 51cm (25^{th}-50^{th} centile). Craniofacial anomalies included mildly turricephalic skull, arched eyebrows, bilateral eyelid ptosis, long eyelashes, long phyltrum, a large and protruding tongue, and gingival hypertrophy with unerupted upper incisors. The nose appeared very soft at palpation. Limbs showed anonychia of the thumbs and great toes, hypoplasia of nails of the 5^{th} fingers and 4^{th} left finger. The remaining toenails were rudimentary. Pectus carinatum, thoracic kyphosis and cervical hirsutism were also noted. Neurologic examination revealed increased drooling, facial expressionless, limb hypotonia and hypotrophic skeletal musculature. He was definitely assessed as affected by severe cognitive and motor disability (Castori *et al.,* 2013).

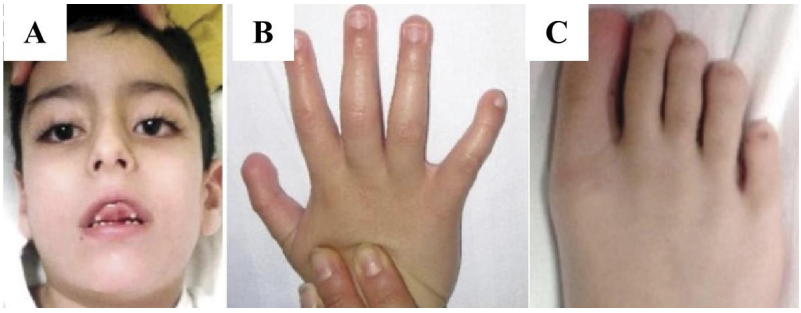

Figure 3. (A-C) **CASE 1**. Pictures showing facial appearance and gingival enlargement (A), anonychia of the thumbs and great toes and nail hypoplasia of the right fifth finger and right second to fifth toes (B, C).

Case 2 (figure 4) was the unique female child of an Italian healthy and unrelated couple (30-year-old mother and 32-year-old father). She was born at term (39 weeks) from normal delivery. Birth parameters were length 48cm (25th centile), weight 2800g (9th-25th centile) and OFC 31cm (0.4th-2nd centile). At birth, generalized hypotonia, coarse face, hirsutism, and partial anonychia of hands and feet were noted. Transfontanellar ultrasound showed periventricular hyperechogenicity. Hand and foot radiographs, performed at 2 months, showed absence of the 2nd and 4th-5th distal phalanges on both hands, absence of 3rd distal phalanx on the left, severe hypoplasia with triangular aspect of 3rd distal phalanx on the right, tapering and mild hypoplasia of 1st distal and 2nd-5th middle phalanges on both hands, absence of 2nd-5th distal and 5th middle phalanges, and hypoplasia of 1st distal and 2nd-4th middle phalanges on both feet. Psychomotor development was delayed as she stood up head at 12 months, sat steady at 24 months, walked with support at 36 months, walked alone at 42 months, said first words at 18 months and first three-word sentences at 5 years. The last neurologic examination, at 5 years and 2 months, better characterized the intellectual disability as borderline (IQ 74) and noted that her communication competence and praxis were delayed, both corresponding to 33 months. The patient underwent standard karyotyping and CGH array with negative results. At examination, patient's weight was 30kg (>97th centile), height 115cm (50th-75th centile) and OFC 51cm (50th centile). Facial features included widow's peak, thick and laterally flared eyebrows, long eyelashes, mildly upslanting palpebral fissures, prominent nasal septum with hypoplastic alae nasi and a vertical cutaneous-cartilagineous ridging on the nasal tip, prominent phyltrum, thick helices and ear lobules. Intraoral examination showed gingival hypertrophy of the upper and lower alveoli with normally erupted decidual teeth. The nose and ear cartilages were extremely soft at palpation. Hands and feet showed complete anonychia. The neck was short. The thumbs were elongated. Hirsutism was evident at back, and upper and lower limbs. The patient also displayed mild hypotonia and generalized joint hypermobility (Castori *et al.,* 2013).

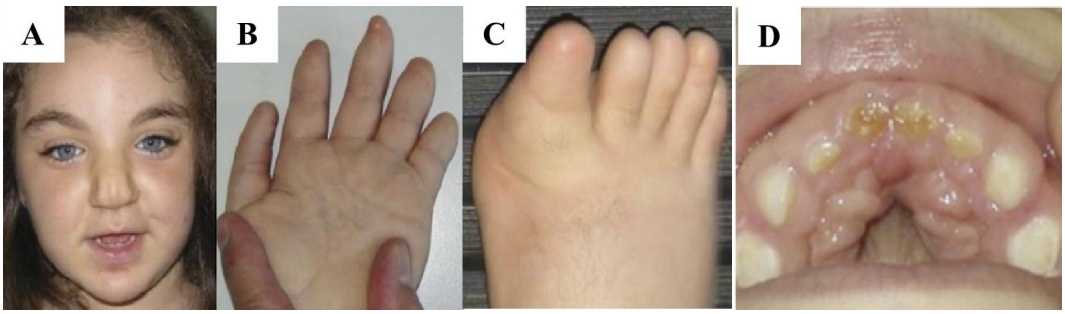

Figure 4. (A-D) CASE 2. Pictures showing facial appearance and gingival enlargement (A,D), anonychia of the fingers of hands and feet, and hypoplasia of the terminal phalanges (B,C).

Case 3 (figure 5) was the first daughter of two Italian non-consanguineous and healthy parents. At birth her weight was 3070g (52th centile), and length was 51cm (84th centile). The OFC measurement is not reported. At examination she was 12 years old, and her parameters were weight 62.5kg (96th centile), height 155cm (71th centile), and OFC 56cm (97th centile). IQ test gave a low score, 55. At 6 months she started with episodes of focal epilepsy, controlled with Tegretol, and electroencephalographic exam showed bilateral frontotemporal abnormal slow electric activity. Ophthalmological examination demonstrated the presence of myopia and oculomotor apraxia. Facial characteristics included thick eyebrows, large nose, bulbous nasal tip, thick helix, macrostomia, thick upper and lower lip, malocclusion and low frontal hairline. Oral examination showed the gingival hyperplasia before anticonvulsant treatment. Limbs were asymmetric. She has scoliosis and moderate hirsutism on limbs. Other features were ataxia, intentional tremor, motor clumsiness, and two café-au-lait spots.

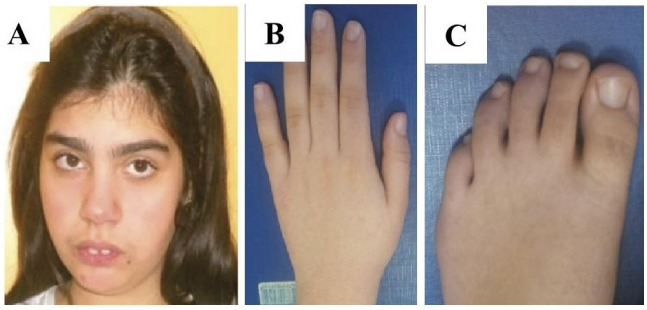

Figure 5. (A-C) CASE 3. Pictures showing facial appearance (A), absent aplasia of fingers and terminal phalanges of hands and feet (B,C).

The three patients' clinical features highlight the great clinical variability of ZLS phenotype. Intellectual disability ranges from very mild (case 2) to severe intellectual disability (case 1).

Hypotonia is present in two cases (case 1 and 2). Epilepsy is present in cases 1 and 3. Ataxia was present in two cases (case 1 and 3). Gingival hyperplasia was present in all the three patients, while hypoplasia of nails and terminal phalanges were present only in cases 1 and 2. The three patients share a coarse face with anomalies of ears and nose cartilages, with a more pronounced phenotype in case 2, showing a peculiar nose (figure 4A). Hirsutism was present in all affected subjects. The comparison among the first three patients studied in this research project is summarized in table 6.

Subject	Case 1	Case 2	Case 3
Sex	**M**	**F**	**F**
ID	+++	+	++
Seizures	+	−	+
Hypotonia	+	+	-
Hearing loss	**NA**	−	**NA**
Coarse face	+	++	+
Gingival enlargement	+	+	+
Aplastic/hypoplastic nails	+	+	−
Aplastic/hypoplastic terminal phalanges	+	+	−
Scoliosis	+	**ND**	+
Hypertrichosis	+	+	+

Table 6. Summary of the features of the first three analyzed patients.
M = male; F = female; + = present; - = absent; ID = intellectual disability; NA = not assessed; ND = not documented.

3.2 Whole-exome sequencing data analysis

WES data analysis allowed to detect a mean coverage of 99.4%, 98.3%, and 99.6% with a mean depth on target of respectively 56x, 57x, and 83x for the three patients, respectively (table 7). The number of total variants identified in the three proband was: 68672, 63874, and 82500, for cases 1, 2 and 3, respectively.

Assuming that this severe phenotype is caused by variants having a great impact on the function of the protein or in the maturation of the transcript, we filtered 10861, 10652, and 10698 high-quality variants with a functional effect (missense, frameshift, stop-gained, stop-loss, start-gained, start-loss, intronic variants located 5 nucleotides from the exon variants), according to UnifiedGenotyper and HaplotypeCaller algorithms.

Since the disease is very rare, we filtered only variants not present, or annotated with a very low frequency in population databases (dbSNP, ExAC and in-house database) narrowing down the number of candidate variants. 348, 310, and 347 variants were selected as novel, clinically associated, or with low/unknown frequency.

Variants were then classified based on genotype (table 7), assuming an autosomal dominant or recessive mode of inheritance.

In case 1, we found one homozygous variant in *KDM6B*, and 32 compound heterozygous variants in 15 genes. For those variants we were not able to predict their phase as we had only sequenced the exome of the proband. For the same reason, it was not possible to assess variants with a *de novo* onset.

In case 2, there were two compound heterozygous variants in *EPPK1*, and one predicted *de novo* variant in *ATP6V1B2* gene.

In case 3, we found 6 predicted compound heterozygous variants in *EVPL*, *KIF7*, and *SNX27*, and 3 predicted *de novo* variants in *EVPL*, *TP53I3*, and *KCNH1* genes.

Case	1	2	3
Target region coverage	99.4%	98.3%	99.6%
Average sequencing depth	56x	57x	83x
Total variants	68672	63874	82500
Nonsynonymous, splice variants (+/-5)	10861	10652	10698
Novel, clinically associated, unknown/low frequency variants	348	310	347
Predicted homozygous variants	1	0	0
Predicted compound heterozygous variants	32[a] (15 genes)	2 (1 gene)	6 (3 genes)
Predicted *de novo* variants	/	1	3

Table 7. Results of the exome sequencing of the first three patients (Cases 1, 2, and 3). Number of variants obtained from the exome sequencing experiments, classified by mode of inheritance. [a]Since we sequenced only the proband, we were not able to establish the phase of those variants.

3.3 Selection of candidate variants

The selection of the candidate variants was based on mode of inheritance, sharing of variants/genes among patients, and deleteriousness of the variants, as described in "Materials and methods" section.

Among all the identified variants, we considered at first the variants/genes shared by at least two patients. This approach led to the identification of three different variants in the same gene (*KCNH1*) in cases 1 and 3. Case 1 carried two variants in heterozygosis, c.125T>C (p.I42T), and c.1054C>G (p.L352V), case 2 c.1405G>A (p.G469R) (NM_002238, NP_002229). The c.125T>C (p.I42T) variant in *KCNH1* was annotated in ExAC with a minor allele frequency of 0.0008% (rs772076205). In case 2, the best candidate variant was a predicted *de novo* variant in *ATP6V1B2* gene, c.1454G>C (p.R485P) (NM_001693, NP_001684) (table 8).

Case	Zygosity	Gene	Genomic position	Nucleotide Change	Amino acid Change	rs ID
1	Compound Heterozygous	*KCNH1*	Chr1:211280674	c.125T>C	p.I42T	rs772076205
			Chr1:211093309	c.1054C>G	p.L352V	.
2	*De novo*	*ATP6V1B2*	Chr8:20077831	c.1454G>C	p.R485P	.
3	*De novo*	*KCNH1*	Chr1:210977485	c.1405G>A	p.G469R	.

Table 8. Selected candidate variants. The mode of inheritance, the genomic position and the variant position on the transcript and protein are indicated.

All the above mentioned variants in the *KCNH1* and *ATP6V1B2* genes were predicted to be "probably damaging" by Polyphen, "damaging" by SIFT, and the CADD score predicted a deleterious effect (table 9).

Case	Gene	Nucleotide change	Amino acid change	Polyphen prediction	SIFT prediction	CADD score
1	*KCNH1*	c.125T>C	p.I42T	Probably damaging	Damaging	27
		c.1054C>G	p.L352V	Probably damaging	Damaging	25.3
2	*ATP6V1B2*	c.1454G>C	p.R485P	Probably damaging	Damaging	34
3	*KCNH1*	c.1405G>A	p.G469R	Probably Damaging	Damaging	34

Table 9. Predicted effect of the candidate variants is summarized, as evaluated by Polyphen, SIFT, and CADD.

3.4 Validation of candidate variants

All the selected variants were analyzed in the probands and their parents through Sanger sequencing and their segregation was confirmed.

In case 1, one of the two variants in *KCNH1*, c.125T>C; p.I42T, resulted to be inherited from the mother, while the other, c.1054C>G; p.L352V, resulted to be *de novo*. The germline origin of the *de novo* variants was confirmed through Sanger sequencing on DNA extracted from blood, hair bulb and/or buccal cells (figure 6). The paternity and maternity were confirmed in the three patients.

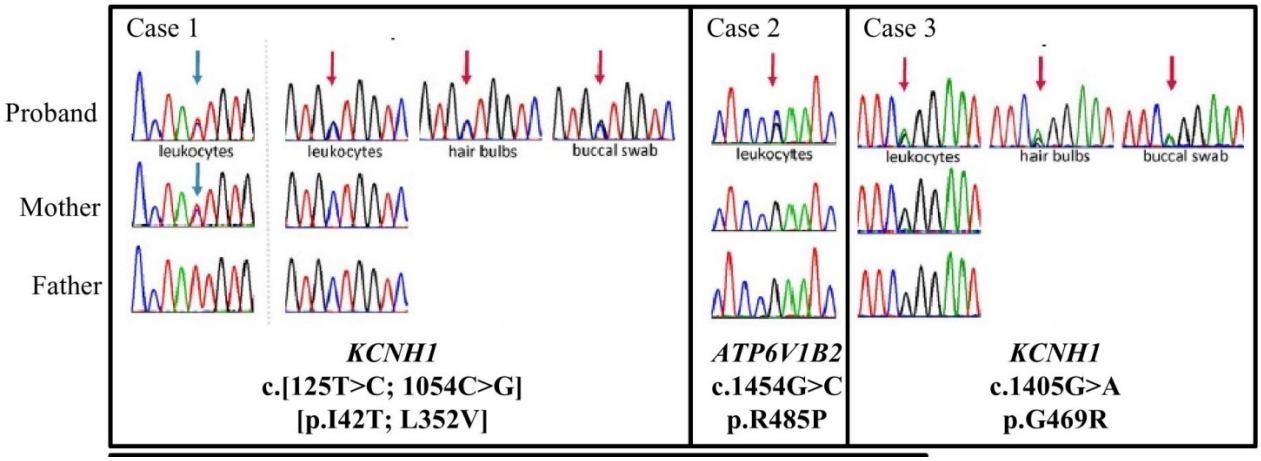

Figure 6. Sequence electropherograms showing the *de novo* origin of the identified *KCNH1* and *ATP6V1B2* missense mutations in cases 1, 2, and 3 (indicated by red arrows). The heterozygous state of three mutations was documented in peripheral leukocytes, hair bulb and/or buccal cells of cases 1 and 3 indicating germline origin. An additional previously annotated heterozygous *KCNH1* variant, c.125T>C (p.Ile42Thr), was present in case 1 and his healthy mother (indicated by blue arrows).

3.5 Haplotype analysis

Case 1 carried two variants in *KCNH1* gene, c.125T>C; p.I42T, inherited from the mother, and c.1054C>G; p.L352V, with a *de novo* onset. In order to characterize the phase of the two variants, amplification of cDNA from patient fibroblasts was performed allowing to detect that the c.125T>C variant was in *cis* with the c.1054C>G variant, demonstrating the onset of the *de novo* variant on maternal allele.

During colony screening through Sanger sequencing a further *KCNH1* isoform, not annotated in EST database (https://www.ncbi.nlm.nih.gov/genbank/) and lacking of exon 6, was identified. Preliminary expression analysis through retrotranscription of RNA from fetal and adult brain and fibroblast suggest that an isoform encompassing exons 1-11 and lacking exon 6 is expressed at least in those tissues. This transcript could potentially lead to the translation of a protein lacking the amino acids 187-344 corresponding to the first three transmembrane helices. Gene expression and biochemical studies are ongoing to better characterize this isoform in terms of expression, localization, and function.

3.6 Enlargement of the ZLS cohort

3.6.1 Clinical features

An international collaboration allowed us to extend the cohort of ZLS patients with 5 further patients. Three of them (cases 5, 6, and 8) were reported by Abo-Dalo and co-workers (2008), while the other two have never been reported before (figure 7). These five patients present the following clinical features:

Case 4: a German girl with severe intellectual disability and autism, hypotonia, generalized tonic clonic seizures, asymmetric cerebral ventricles, macrocephaly, long and coarse face, gingival hyperplasia, hypoplastic terminal phalanges of hands and feet, aplastic or hypoplastic nails, thoracic scoliosis, and hypertrichosis.

Case 5: an Australian boy with profound intellectual disability, hypotonia, seizures, coarse face, thick scalp hair and eyebrows, broad forehead, broad nasal tip, short philtrum, thick lips, large ears with anteverted and thickened ear helices, gingival hyperplasia, aplastic or hypoplastic nails, and severe scoliosis (Abo-Dalo *et al.,* 2008).

Case 6: an Australian girl with profound intellectual disability, hypotonia, seizures, macroglossia, central incisor, arched eyebrows, gingival hyperplasia, hypoplastic terminal phalanges and aplastic nails of hands and feet, and thoracic scoliosis (Abo-Dalo *et al.,* 2008).

Case 7: an Indian female with severe intellectual disability, neonatal seizures, sensorineural hearing loss, bilateral horizontal nystagmus, low set ears, high forehead, pointed nose, prominent alae nasi, mild hypertelorism, epicanthal folds, long philtrum, large lower lips, down turned angle of mouth, hypoplasia of terminal phalanges, and bilateral nail aplasia/hypoplasia.

Case 8: a French boy with severe intellectual disability, hypotonia, encephalopathy, unilateral total deafness, coarse face, thick scalp hair, synophrys, large bulbous nose with "bifid" nasal tip, thick lips, macroglossia, gingival hyperplasia, aplastic terminal phalanges and nails of hands and feet, severe kyphosis/lordosis, and hypertrichosis (Abo-Dalo *et al.,* 2008).

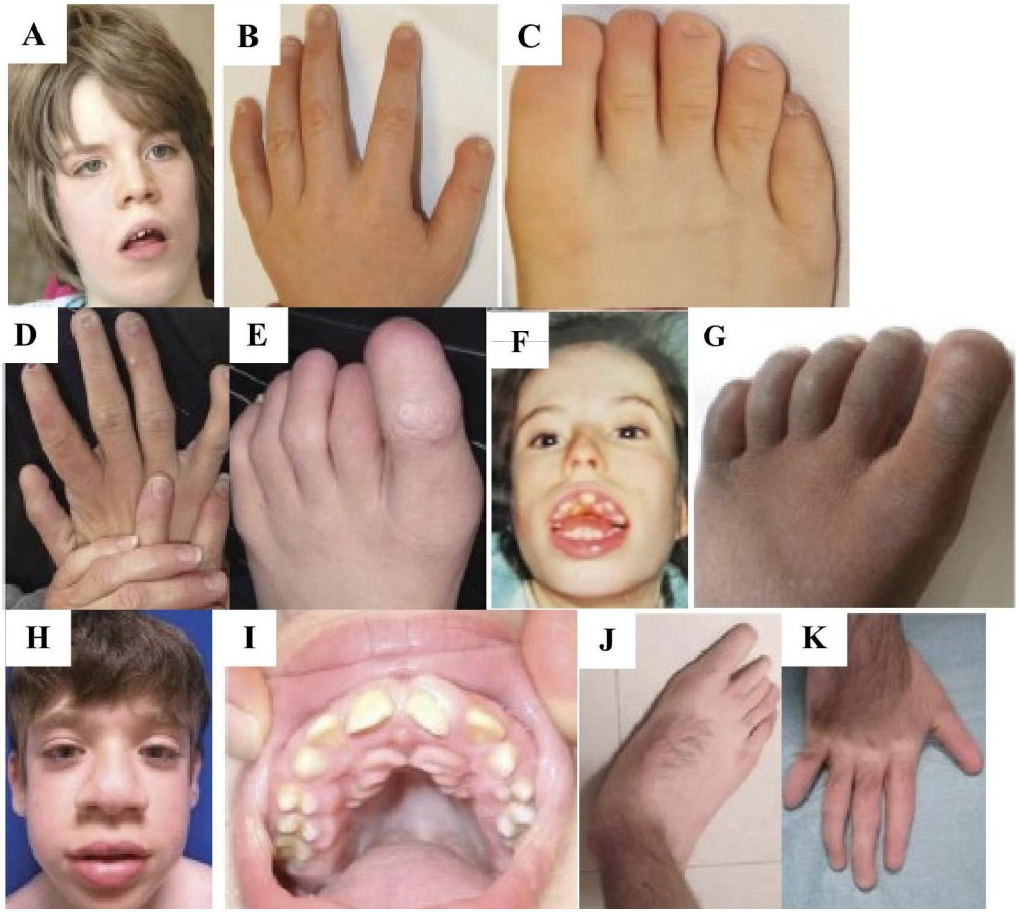

Figure 7. Clinical features of the additional ZLS-affected individuals (**A**, **F**) Facial phenotype of cases 4, 6, and 8: (**A**) case 4, (**F**) case 6, (**H**) case 8. Note the gingival enlargement in case 6. (**B**, **C**) Case 4 shows anonychia of the right great toe and hypoplastic nails of all other right toes and fingers of left hand. (**D**, **E**) Case 5 shows aplastic nails of the thumb and first to third toes and hypoplastic nails of all other fingers and toes. (**G**) Case 7 shows anonychia of the left great toe and hyponychia of all other toes. (**I**) Gingival enlargement in case 8. (**J**, **K**) Case 8 shows aplastic terminal phalanges of the second and fifth fingers on the left hand, the fifth finger on the right hand and all toes except the first. Hypertrichosis can be observed in case 8 (**J**, **K**).

3.6.2 Whole-exome sequencing results

WES was performed on cases 4 and 8 and data analysis allowed to detect a mean coverage of 97.7%, and 98.6% with a mean depth on target of respectively 36x, and 52x for the two patients,

respectively. Among the total variants (70894, and 81294), 9542, and 10693 high-quality variants with a functional effect (missense, frameshift, stop-gained, stop-loss, start-gained, start-loss, intronic variants located 5 nucleotides from the exon variants) were predicted by UnifiedGenotyper and HaplotypeCaller algorithms for each case. After frequency filtering, 227, and 268 were selected as novel, clinically associated, or with low/unknown frequency. Variants were then classified based on genotype. In case 4, we found two predicted homozygous variants in *IL4R*, and *CAPN15*, 4 predicted compound heterozygous variants in *DNMBP* and *RGS3*, and 6 predicted *de novo* variants in *IKZF2*, *CLK4*, *SDK1*, *SLC38A2*, *VPS13C*, and *KCNH1*.

In case 8, there were 4 predicted compound heterozygous variants in *CPXM2*, and *HSPG2*, and 7 predicted *de novo* variant in *CFHR5, PMS2, TJP2, DNAJC25-GNG10, NAV3, GP1BA*, and *ATP6V1B2* (table 10).

Case	4	8
Target region coverage	97.7%	98.6%
Average sequencing depth	36x	52x
Total variants	70894	81294
Nonsynonymous, splice variants (+/-5)	9542	10693
Novel, clinically associated, unknown/low frequency variants	227	268
Predicted homozygous variants	2	0
Predicted compound heterozygous variants	4 (2 genes)	4 (2 genes)
Predicted *de novo* variants	6	7

Table 10. Results of the exome sequencing of cases 4 and 8. Number of variants obtained from the exome sequencing experiments, classified by mode of inheritance.

3.6.3 Selection of candidate variants

The selection of the candidate variants was based on mode of inheritance, sharing of variants/genes among patients, and deleteriousness of the variants.

Among all the identified variants, we considered at first the variants/genes shared with the previously analyzed exomes. This approach led to the identification of a variant in *KCNH1* gene in case 4, c.1399A>G (p.I467V) (NM_002238, NP_002229). The variant found in *KCNH1* has never been reported in dbSNP or ExAC. In case 8, the same variant in *ATP6V1B2* found in case 2, c.1454G>C (p.R485P) (NM_001693, NP_001684) was identified (table 11).

Case	Zygosity	Gene	Genomic position	Nucleotide change	Amino acid change	rs ID
4	*De novo*	*KCNH1*	Chr1:210977491	c.1399A>G	p.I467V	.
8	*De novo*	*ATP6V1B2*	Chr8:20077831	c.1454G>C	p.R485P	.

Table 11. Selected candidate variants. The mode of inheritance, the genomic position and the variant position on the transcript and protein are indicated.

3.6.4 Validation of candidate variants and Sanger sequencing screening

All the selected variants were analyzed in the probands and their parents through Sanger sequencing and their segregation was confirmed.

The variant found in case 4 in *KCNH1* gene, c.1399A>G; p.I467V, and the variant identified in case 8 in *ATP6V1B2* gene, c.1454G>C; p.R485P, resulted to be *de novo* (figure 8). The paternity and maternity were confirmed in the two patients.

In addition, a Sanger sequencing screening of the coding sequences of *KCNH1* and *ATP6V1B2* genes in the cases 5, 6, and 7 allowed us to identify a patient with two new *de novo* variants *in cis*, c.[974C>A;1066G>C], p.[S325Y;V356L], one patient with one new *de novo* variant, c.1042G>A (p.G348R), and one patient with a *de novo* variant already identified, c.1399A>G (p.I467V) in case 4, in *KCNH1* (figure 8 and 9). Those variants resulted not to be annotated in dbSNP and ExAC (table 12).

Case	Zygosity	Gene	Genomic position	Nucleotide change	Amino acid Change	rs ID
5	*De novo*	*KCNH1*	Chr1:211093389; 211093297	c.[974C>A; 1066G>C]	p.[S325Y; V356L]	.
6	*De novo*	*KCNH1*	Chr1:211093321	c.1042G>A	p.G348R	.
7	*De novo*	*KCNH1*	Chr1:210977491	c.1399A>G	p.I467V	.

Table 12. Variants identified in cases 5, 6 and 7 through Sanger sequencing screening of the coding sequence of *KCNH1* and *ATP6V1B2* genes. The mode of inheritance, the genomic position and the variant position on the transcript and protein are indicated.

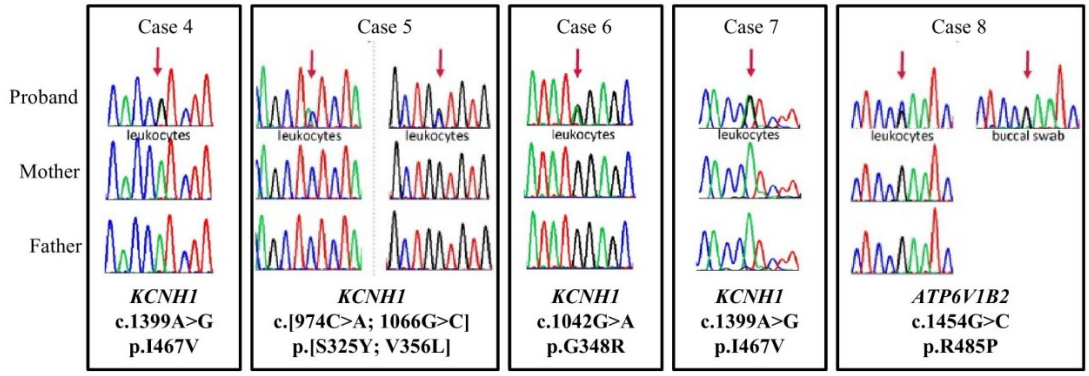

Figure 8. Sequence electropherograms showing the *de novo* origin of the identified *KCNH1* and *ATP6V1B2* missense mutations in cases 4-8 (indicated by red arrows). The heterozygous state of three mutations was documented in peripheral leukocytes for all samples and in buccal cells in case 8.

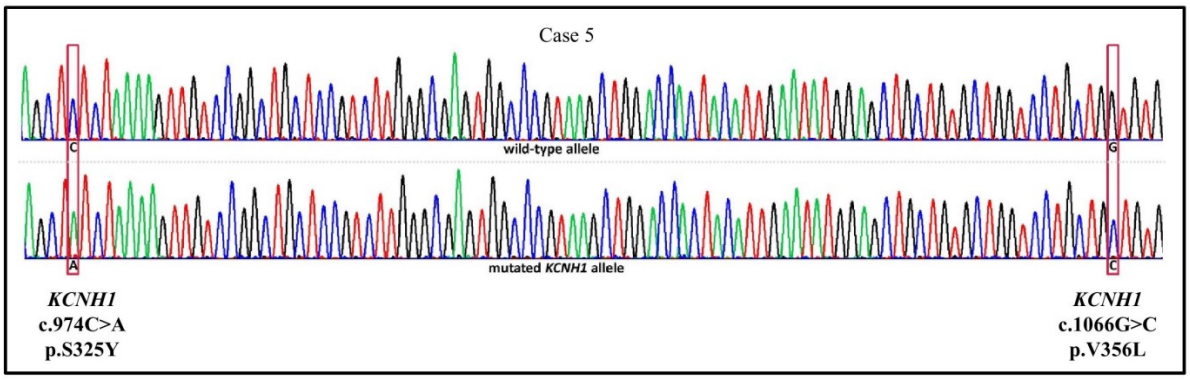

Figure 9. By cloning the *KCNH1* exon 7–containing amplicon of case 5 followed by sequencing, we determined the haplotypes and found that the two identified *de novo* changes c.974C>A and c.1066G>C are in *cis* (wild-type allele above, and mutated *KCNH1* allele below in the figure; mutated nucleotides are framed).

The c.1399A>G (p.I467V) variant in *KCNH1* was predicted to be "probably damaging" by Polyphen, and deleterious according to CADD score. SIFT predicted this variant as "tolerated". The c.974C>A (p.S325Y) variant in *KCNH1* was predicted as "possibly damaging" by Polyphen, "damaging" by SIFT and deleterious by the CADD scoring system. The c.1066G>C (p.V356L) variant in *KCNH1* was predicted as "benign" by Polyphen, "tolerated" by SIFT, and deleterious according to the CADD score. Finally, the c.1042G>A (p.G348R) variant in *KCNH1* was predicted as "probably damaging" by Polyphen, "damaging" by SIFT, and deleterious by the CADD score (table 13).

Case	Gene	Nucleotide Change	Amino acid Change	Polyphen prediction	SIFT prediction	CADD score
4, 7	*KCNH1*	c.1399A>G	p.I467V	Probably damaging	Tolerated	24.7
5	*KCNH1*	c.974C>A	p.S325Y	Possibly damaging	Damaging	24.6
		c.1066G>C	p.V356L	Benign	Tolerated	21.9
6	*KCNH1*	c.1042G>A	p.G348R	Probably damaging	Damaging	31

Table 13. Predicted effect of the mutations identified in the patients enclosed in the enlarged cohort is summarized, as evaluated by Polyphen, SIFT, and CADD.

All the identified variants were highly conserved across eukaryotes, figure 10.

Figure 10. Multiple protein sequence alignments around the KCNH1 and ATP6V1B2 amino acid substitutions from different species. Alignment of the regions flanking the detected missense variants in orthologous proteins, showing the evolutionary conservation of amino acids S325, G348, L352, V356, I467 and G469 in human KCNH1 (NP_002229) and of R485 in human ATP6V1B2 (NP_001684). Multiple alignments were gathered from http://www.ncbi.nlm.nih.gov/homologene/. Conserved residues have a red background, and non-conserved residues have a gray background. Amino acid sequence alignments demonstrate high (S325 and V356 in human KCNH1) or complete (G348, L352, I467 and G469 in human KCNH1 and R485 in human ATP6V1B2) evolutionary conservation of the altered residues.

3.7 ZLS cohort: summary of the clinical features

All the patients analyzed through WES and Sanger sequencing and found to be mutated in *KCNH1* and *ATP6V1B2* genes show intellectual disability, and coarse face. Deafness was present in 2/8 cases, gingival hyperplasia and hypoplastic nails/phalanges in 7/8 cases, scoliosis in 6/8 cases,

hirsutism in 5/8 (tables 14 and 15). Worth to be noted, seizures is present only in the six patients harboring *KCNH1* mutations (table 14). The two patients (cases 4 and 7) with the c.1399A>G (p.I467V) variant in *KCNH1* have in common severe intellectual disability, seizures, a coarse face, and hypoplastic nails and phalanges, the hypoplasia of phalanges is less marked in case 7 than in case 4. The two patients mutated in *ATP6V1B2* (case 2 and 8) both have intellectual disability, a very similar coarse face, gingival hyperplasia, hypoplastic nails and phalanges, and marked generalized hirsutism. Intellectual disability was mild in case 2 and severe in case 8, gingival hyperplasia was less marked in case 2 than in case 8.

Gene	***KCNH1***					
Mutation (NM_002238)	**c.1054C>G p.L352V**	**c.1405G>A p.G469R**	**c.1399A>G p.I467V**		**c.[974C>A;1066G>C] p.[S325Y;V356L]**	**c.1042G>A p.G348R**
Mutation (NM_172362)	**c.1135C>G p.L379V**	**c.1486G>A p.G496R**	**c.1480A>G p.I494V**		**c.[1055C>A;1147G>C] p.[S352Y;V383L]**	**c.1123G>A p.G375R**
Case	**1**	**3**	**4**	**7**	**5**	**6**
Sex	**M**	**F**	**F**	**F**	**M**	**F**
ID	+	+	+	+	+	+
Seizures	+	+	+	+	+	+
Hypotonia	+	-	+	-	+	+
Deafness	**NA**	**NA**	-	+	-	-
Coarse face	+	+	+	+	+	+
Gingival hyperplasia	+	+	+	-	+	+
Hypoplastic nails	+	-	+	+	+	+
Hypoplastic phalanges	+	-	+	+	-	+
Scoliosis	+	+	+	**ND**	+	+
Hirsutism	+	+	+	-	-	-

Table 14. Summary of the mutations identified in *KCNH1* in this work (reported in Kortum *et al*., 2015), and clinical features of the analyzed patients. Mutations are reported according to both the isoforms.
M = Male, F = Female, ID = Intellectual Disability, NA = Not Assessed, ND = Not Documented

Gene	*ATP6V1B2*	
Mutation (NM_001693)	**c.1454G>C p.R485P**	
Case	**2**	**8**
Sex	**F**	**M**
ID	+	+
Seizures	-	-
Hypotonia	+	+
Deafness	-	+
Coarse face	+	+
Gingival hyperplasia	+	+
Hypoplastic nails	+	+
Hypoplastic phalanges	+	+
Scoliosis	-	+
Hirsutism	+	+

Table 15. Summary of the mutations identified in *ATP6V1B2* in this work (reported in Kortum *et al*., 2015), and clinical features of the analyzed patients. M = Male, F = Female, ID = Intellectual Disability

3.8 *KCNH1*: structural and functional studies results

The *KCNH1* gene is located on the long arm of chromosome 1. Alternative splicing of this gene results in two transcript variants encoding distinct isoforms (NM_172362 and NM_002238), that differ in the coding sequence for 81 nucleotides in length. The encoded protein is a member of the potassium channel, voltage-gated, subfamily H protein (also called K_v10.1). This member is a pore-forming subunit of a voltage-gated non-inactivating delayed rectifier potassium channel. The functional channel is a homotetramer constituted by 7 transmembrane helices, and a hairpin structure (known as the pore-forming loop, P-loop). It is highly expressed in myoblast and brain, and activates at the onset of myoblast differentiation. Five of six mutations that we found in ZLS patients are located in the two helices involved in the opening of the channel, one mutation maps in the voltage-sensor helix (figure 11).

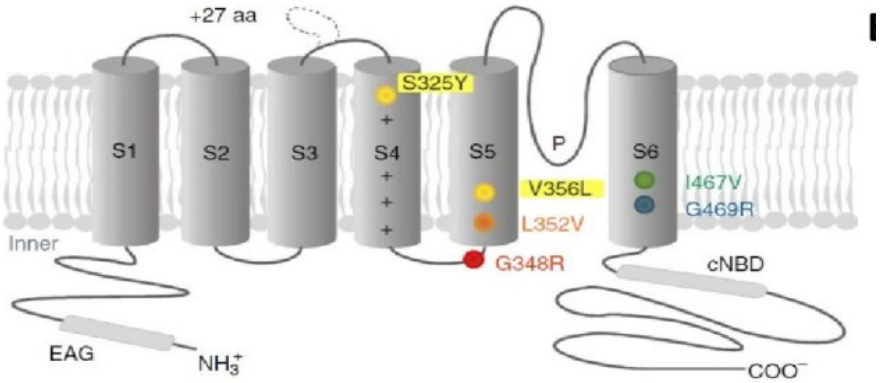

Figure 11. Schematic view of the KCNH1 channel showing the location of the residues affected in individuals with ZLS (colored dots). The S4 segment acts as voltage-sensor domain, and the assembly of four subunits is required to form a functional channel. cNBD, cyclic nucleotide-binding domain; EAG, EAG domain; P, pore region

In collaboration with Prof. Lorenzo Stella's research group of Tor Vergata, the KCNH1 mutations were characterized from the structural point of view using a homology model. The affected amino acid residues of KCNH1 were located in the voltage-sensing S4 helix (S325), the S4–S5 linker (G348), and the S5 (L352 and V356) and S6 (I467 and G469) segments. The p.G469R change is predicted to impair tetramer formation or favour the open state with a lower conductance due to the presence of cationic residues close to the channel pore. L352, V356 and I467 form a tight hydrophobic cluster in the open structure, which rearranges in the closed conformation. Perturbations of these residues, are predicted to affect the closed/open transition (figure 12).

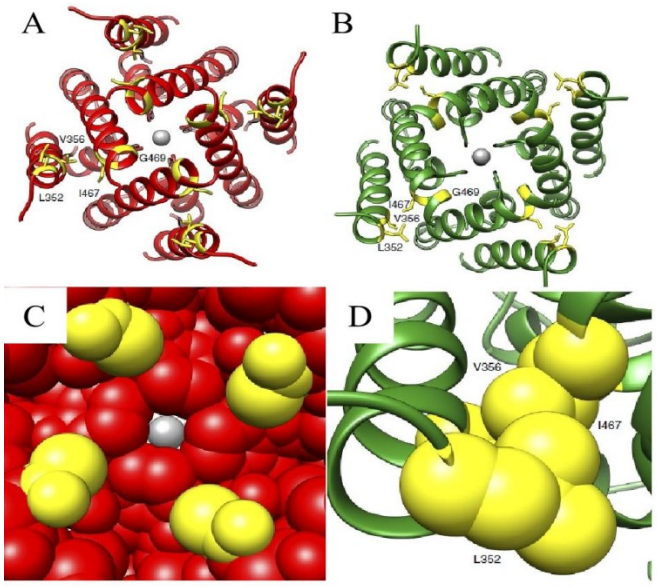

Figure 12. Structural impact of ZLS-associated *KCNH1* mutations. (**A**) Model of helices S5 and S6 of KCNH1 in their closed state (viewed from the intracellular side of the membrane). Affected residues (yellow) and K^+ (gray sphere) are shown. (**B**) Model of helices S5 and S6 of KCNH1 in their open state. The color code is as in **a**. (**C**) Enlargement of the pore-closing region in the closed state. Atoms are shown as spheres to illustrate the steric hindrance of this region, which would hardly accommodate a larger charged residue, such as arginine, at position 469. (**D**) Enlargement of the hydrophobic cluster formed by L352, V356 and I467 (side chains shown in sphere representation) in the open state.

In collaboration with a research group of the University of Hamburg, functional consequences of the ZLS-associated *KCNH1* mutations by patch-clamp experiments on CHO cells expressing wild-type and mutant KCNH1 channels were assessed. The current amplitudes of the mutants did not differ significantly from the amplitudes of wild-type KCNH1; all mutant channels, however, exhibited a remarkable shift in the activation threshold to more negative potentials, producing dramatic increases in whole-cell K^+ conductance in the negative-potential range (the G469R change gives this result when the mutated protein is co-expressed with the wild type protein). In comparison to wild-type channels, the mutants exhibited accelerated channel activation and slower deactivation. Together, these data show a potential gain-of-function effect for the disease-associated KCNH1 mutants (figure 13).

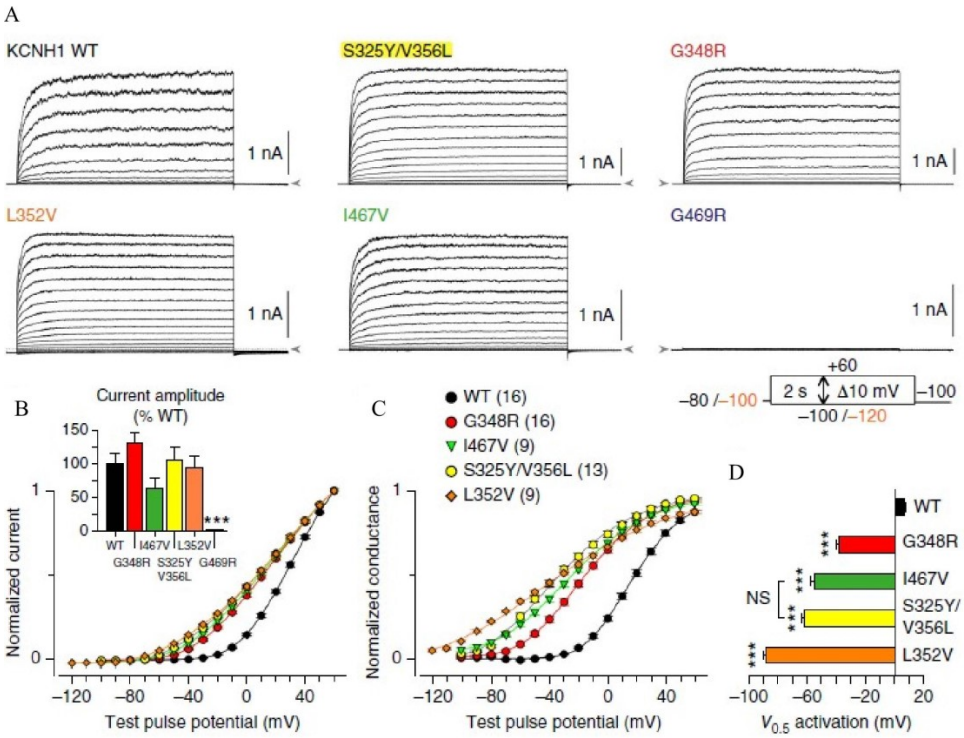

Figure 13. Voltage-dependent activation of human wild-type (WT) and mutant KCNH1 channels expressed in CHO cells. (**A**) Families of whole-cell currents elicited with 2-s variable test pulses as indicated in the pulse protocol shown at the right below the current traces. For the L352V mutant, a more negative holding potential of −100 mV and test pulses starting from −120 mV were used. Expression of the G469R mutant did not result in recordings of voltage-dependent K^+ currents (n = 22). Zero current is indicated by dashed lines and arrowheads. (**B**) Mean (±s.e.m.) KCNH1 current amplitudes as a function of the test pulse potential. Current amplitudes were normalized to the maximum amplitude recorded at +60 mV. Data points were connected by straight lines. The inset shows current amplitudes at +40 mV normalized to the mean current for the wild-type channel. (***P < 0.001, significantly different from wild type) (**C**) Mean (±s.e.m.) normalized whole-cell conductance as a function of the test pulse potential. Lines represent fourth-order Boltzmann functions fitted to the data points. Numbers of experiments are shown in parentheses. (**D**) Mean (+s.e.m.) values of the potential of half-maximal KCNH1 channel activation (V0.5 activation), derived from fits to permeability data considering the Goldman-Hodgkin-Katz current equation. One-way ANOVA with *post-hoc* Bonferroni t testing yielded significant (***P < 0.001) differences for all combinations except the one indicated (NS, not significant).

3.9 *ATP6V1B2:* 3D studies results

The *ATP6V1B2* (ATPase H^+ Transporting V_1 Subunit B2) gene encodes a non-catalytic subunit of the peripheral V_1 complex of vacuolar ATPase, a multisubunit enzyme that mediates acidification of eukaryotic intracellular organelles, and is located on the short arm of the chromosome 8. V-ATPase is composed of a cytosolic V_1 domain and a transmembrane V_0 domain. The V_1 domain contains the ATP catalytic site. The p.R485P mutation falls at the interface between subunits B and A (figure 14).

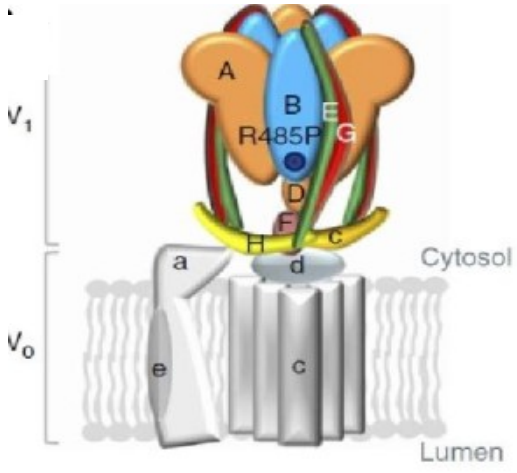

Figure 14. Schematic view of the subunit structure of the V-ATPase. The catalytic V_1 complex consists of the A, B, C, D, E, F, G and H subunits. The V_0 domain is membrane embedded and is composed of a characteristic C-ring structure with which the a, d and e subunits are associated. R485 is highlighted by a blue dot.

To explore the structural impact of the p.R485P amino acid change a homology model of the B2 subunit was generated and inserted into the crystallographic structure of the A_3B_3 hexamer of the *Enterococcus hirae* ATPase. p.R485P substitution is not expected to affect the affinity of the protein for the ATP. R485 is however located in an α-helical segment that is predicted to be disrupted by substitution to proline. Overall, the arginine-to-proline substitution is predicted to perturb intersubunit interactions within the V_1 subcomplex by destabilizing the C-terminal segment of the B subunit (figure 15).

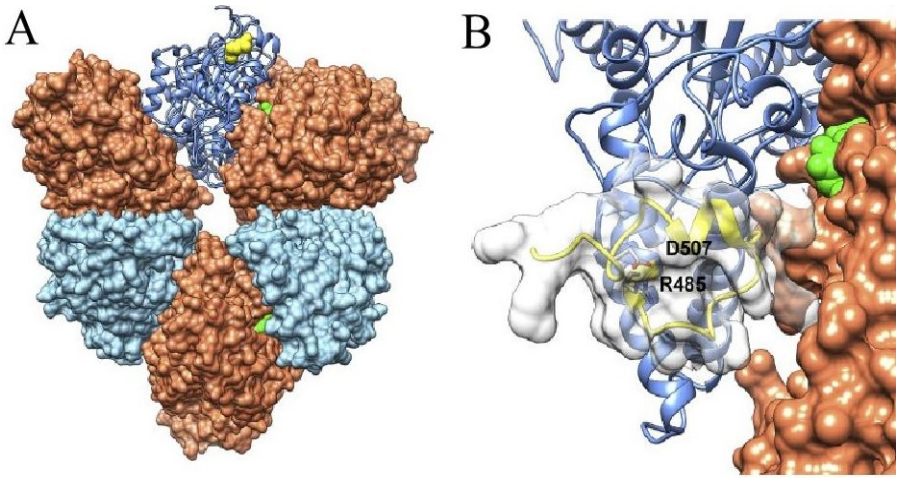

Figure 15. Structural impact of ZLS-associated *ATP6V1B2* mutation. (**A**) Homology model of the B subunit of the human V-ATPase (ribbon representation) in the context of the A_3B_3 hexamer of the *E. hirae* ATPase (surface representation, with A subunits colored in salmon and B subunits colored in light blue). The complex is shown as seen from the membrane surface. One of the B subunits was substituted by the homology model of the B subunit of the human V-ATPase (ribbon representation). ATP analogs are shown in green, and R485 is represented in yellow. (**B**) Enlargement of the A-B interface. R485 and D507 are shown in stick representation. The C-terminal segment of the B subunit predicted to be destabilized by the p.R485P substitution is represented in yellow. The space-filling model of residues 485–511 is also shown, as a semitransparent white surface.

3.10 Further ZLS cohort enlargement

With the aim of disclosing the presence of additional *KCNH1*/*ATP6V1B2* mutations or new genes mutated in patients with features of ZLS phenotypic spectrum and to better characterize molecular bases, we recruited 4 additional patients. These patients have clinical features strongly suggestive of ZLS, like coarse face, gingival hyperplasia, hypertrichosis, aplasia/hypoplasia of nails and terminal phalanges.

Sanger sequencing screening of the entire coding sequences of *KCNH1* and *ATP6V1B2* genes in the probands resulted to be negative, suggesting genetic heterogeneity.

Therefore, we decided to perform a WES approach in two patients (case 9 and 10) and their respective parents (figures 16 and 17). While in case 10 the WES data analyses are still ongoing, for the case 9, results are reported in the following section.

Case 9 has intellectual disability, a bulbous soft nose with a bifid tip, malformation of the cartilage ears, nail aplasia of hands and feet, and hypoplastic terminal phalanges. Worth of noting, the father presented some clinical features present in his daughter but in a milder form, as a bulbous nose, and hypoplastic nails and terminal phalanges of hands and feet (figure 16).

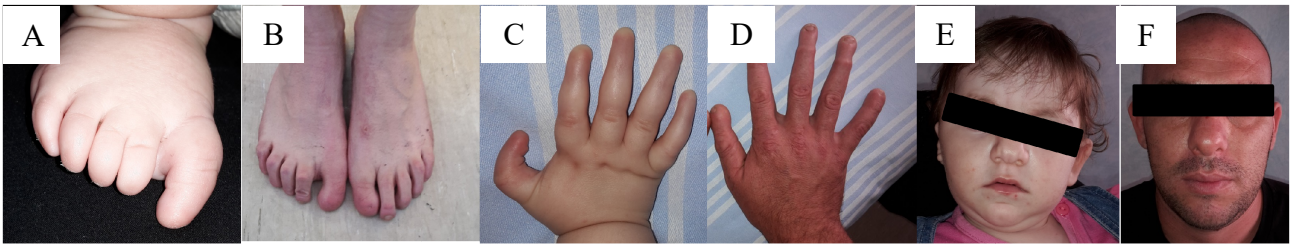

Figure 16. Comparison among phenotypic features of case 9 and her father. Feet and hands of case 9 (A,C) show complete lack of nails, while father's feet and hands show hypoplastic nails (B,D). The nose shape of the proband (E) and her father (F) are very similar.

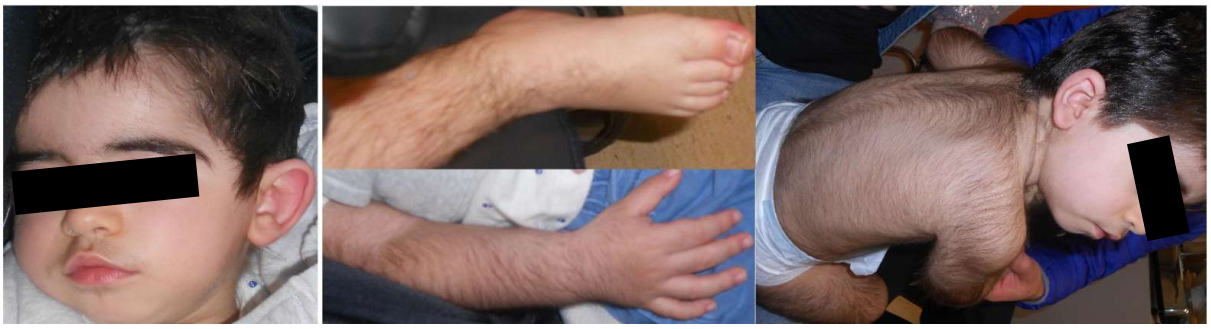

Figure 17. Pictures showing some of the features of case 10. Long eyebrows, mild facial hypertrichosis, downturned corners of the mouth, limbs and back hypertrichosis.

3.11 WES data analysis results

WES data analysis of case 9 allowed to obtain a coverage of 97% of the target regions with a mean depth of 111x. Among the 73379 total variants, 13431 were of high quality and had a functional effect (missense, frameshift, stop-gained, stop-loss, start-gained, start-loss, intronic variants located five nucleotides from the exon variants). 442 were novel, clinically associated, or with low/unknown frequency variants. Variants were then classified based on the genotype, disclosing the presence of six compound heterozygous variants in three genes (*CCDC86*, *DNAH11*, and *SERPINA10*) and four *de novo* variants, in *TMEM247*, *ATP6V1C1*, and *SARAF* genes (table 16).

Case	9
Target region coverage	97%
Average sequencing depth	111x
Nonsynonymous, splice variants (+/-5)	13431
Novel, clinically associated, unknown/low frequency variants	442
Predicted homozygous variants	0
Predicted compound heterozygous variants	6 (3 genes)
Predicted *de novo* variants	4

Table 16. Results of the exome sequencing of case 9. Number of variants identified in the exome, classified by mode of inheritance.

3.12 Variants analysis and selection of candidate genes

Variants and genes identified in the previous step were analyzed in details in order to select the best candidate variant/s. The genes harboring the compound heterozygous variants were excluded for several reasons, i.e. frequency in population database, gene expression and protein function. The *de novo* variants in *SARAF* and *TMEM247* genes were excluded because they were artifacts due to a misalignment of the reads. The best candidate was a predicted *de novo* variant c.865G>A, p.E289K, that affects a highly conserved amino acid in *ATP6V1C1* gene (NM_001695, NP_ 001686) (figure 18), coding for an interactor of ATP6V1B2 subunit (table 17).

Case	Zygosity	Gene	Genomic position	Nucleotide change	Amino acid change	rs ID
9	*De novo*	*ATP6V1C1*	Chr8:104076978	c.865G>A	p.E289K	.

Table 17. New candidate gene identified by WES of the patient added to the ZLS cohort. The mode of inheritance, the genomic position and the variant position on the transcript and protein level are indicated.

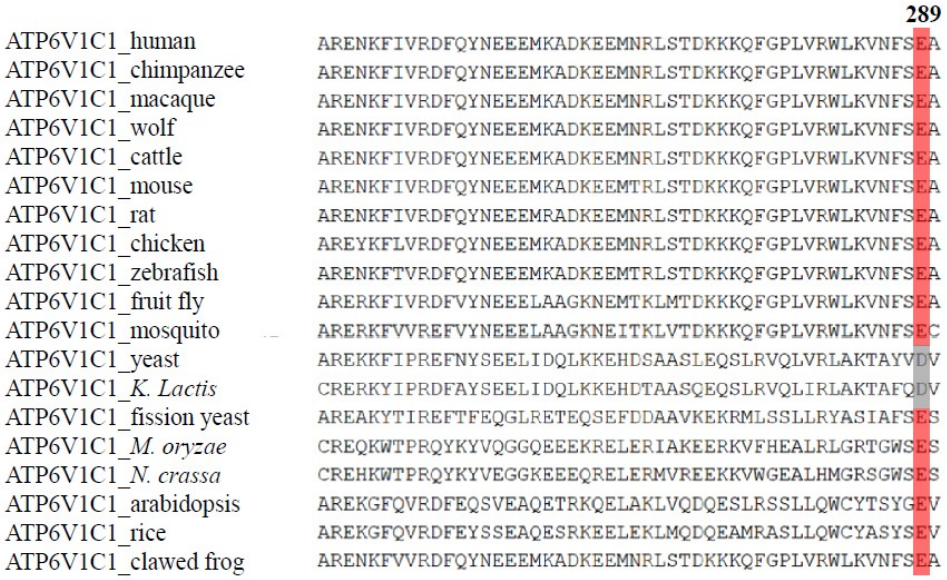

Figure 18. Multiple protein sequence alignments near the ATP6V1C1 amino acid substitution from different species. Alignment of the regions flanking the detected missense variant in orthologous proteins, showing the evolutionary conservation of amino acid E289 in human ATP6V1C1 (NP_001686). Multiple alignment was gathered from http://www.ncbi.nlm.nih.gov/homologene/. Conserved residues have a red background, and non-conserved residues have a gray background. Amino acid sequence alignments demonstrate a highly evolutionary conservation of the altered residue.

This variant was predicted as "possibly damaging" by Polyphen, "damaging" by SIFT, and deleterious according to the CADD score (table 18).

Case	Gene	Nucleotide Change	Amino acid change	Polyphen Prediction	SIFT prediction	CADD score
9	*ATP6V1C1*	c.865G>A	p.E289K	Possibly damaging	Damaging	36

Table 18. Predicted effect of the newly identified variant in case 9 according to Polyphen, SIFT, and CADD.

3.13 Validation of candidate variant

Sanger sequencing confirmed the presence of the variant in the proband in DNA extracted from blood, hair bulb, and buccal cells (figure 19).

The presence in the father of case 9 of some features fitting with ZLS syndrome suggested the presence of the pathogenic variant also in this subject, probably with a lower percentage of cells carrying the mutation.

Electropherograms of the region encompassing *ATP6V1C1* variant of the father disclosed the presence of the variant allele in a low proportion in DNA from different tissues (blood, hair bulb, buccal cells) (figure 19A). A manual inspection, using the Integrative Genomics Viewer (IGV) of reads aligning in this region of father WES, disclosed the presence of 6 reads with the variant allele *versus* 85 reads carrying the wild-type allele (figure 19B). The c.865G>A (p.E289K)

variant was not detected by variant calling algorithms used in the WES analysis pipeline probably due to the low abundance of the variant allele. When we applied a different pipeline (MuTect2, Cibulskis *et al.,* 2013) from the GATK package, a somatic SNP and indel caller that takes into account the presence of mosaicism, the *ATP6V1C1* variant allele was identified also in the father (figure 19B).

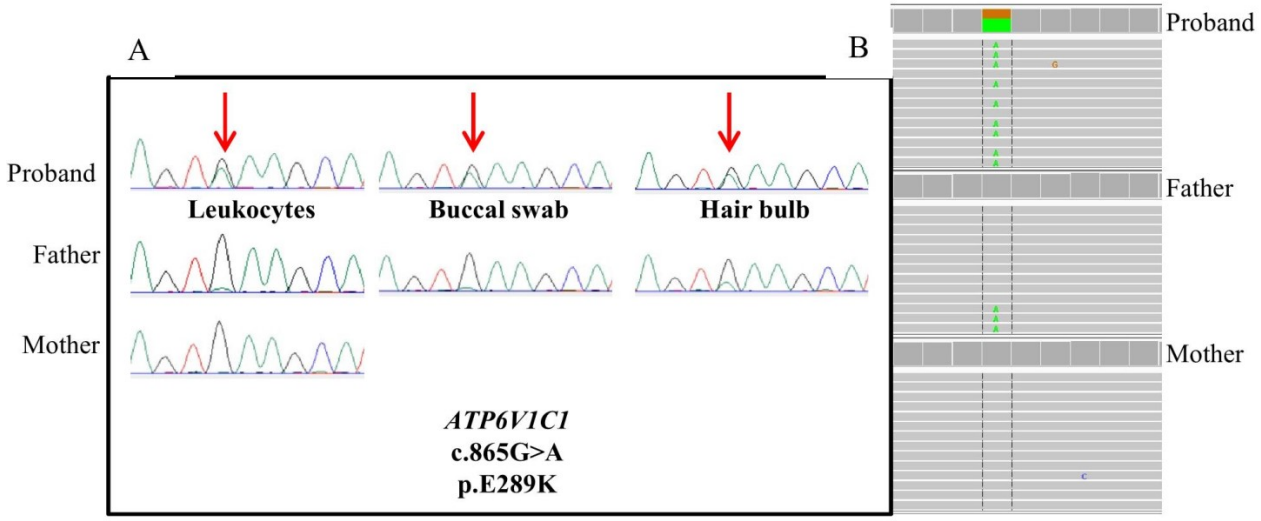

Figure 19. (A) Electropherograms showing the mutation in *ATP6V1C1* gene in the proband's cells and, with variable proportion, also in the father. **(B)** Reads from father WES alignment with IGV disclosing the presence of low copy number reads harboring the variant allele.

3.14 *ATP6V1C1* gene

ATP6V1C1 (ATPase H^+ Transporting V_1 Subunit C1), is located on the long arm of chromosome 8, and encodes a component of vacuolar ATPase (V-ATPase). *ATP6V1C1* is one of two genes encoding the V_1 domain C subunit proteins and is ubiquitously expressed. The subunit C is necessary for the assembly of the catalytic sector of the enzyme and is likely to have a specific function in its catalytic activity. ATP6V1C1 is an essential component of the osteoclast proton pump and in F-actin ring formation in osteoclasts (Feng *et al.,* 2009). In figure 20 the structure of the V-ATPase is represented and the subunit affected by the mutation is indicated.

Structural analyses are ongoing to characterize the effect of the *ATP6V1C1* mutation on the ATPase assembly/function.

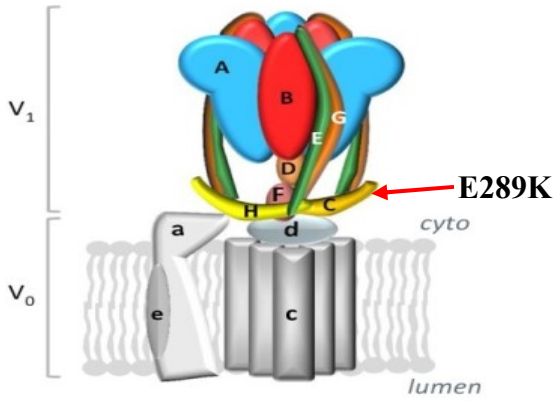

Figure 20. Schematic view of the subunit structure of the V-ATPase. The catalytic V_1 complex consists of the A, B, C, D, E, F, G and H subunits. The V_0 domain is membrane embedded and is composed of a characteristic C-ring structure with which the a, d and e subunits are associated. The subunit affected by the p.E289K is indicated by a red arrow.

4. Discussion

Zimmermann-Laband Syndrome (ZLS), firstly described in 1928 by Zimmermann, is characterized by gingival fibromatosis, dysplastic or absent nails, hypoplasia of the distal phalanges, scoliosis, hepatosplenomegaly, hirsutism, and abnormalities of the cartilage of the nose and/or ears. To date, about 40 patients have been described with features fitting ZLS.

ZLS belongs to a group of clinically overlapping and genetically heterogeneous syndromes, such as Temple-Baraitser syndrome (TMBTS), dominant deafness-onychodystrophy syndrome (DDOD), deafness, onychodystrophy, osteodystrophy, mental retardation, seizures syndrome (DOORS), and Cantu syndrome (CS). Intellectual disability, epilepsy, deafness, hypoplasia or aplasia of nails and/or terminal phalanges, and gingival enlargement vary among the different disorders as well as within each condition.

With the aim of identifying ZLS causative gene/s, we selected three patients with the diagnosis of Zimmermann-Laband syndrome and performed a WES approach on the three patients and their parents in two cases. DNA variants were analyzed and prioritized based on segregation, sharing among patients, effect on protein structure/function and gene function. This analysis let us to identify two excellent candidate genes, *KCNH1* and *ATP6V1B2*. An enlargement of the cohort was performed through the recruitment of further five patients in a collaborative effort with several international research groups. Patients were analyzed by WES or Sanger sequencing of the coding portion of *KCNH1* and *ATP6V1B2* genes confirming the presence of additional mutations.

Overall, this analysis led to the identification of six mutations in *KCNH1* gene in six patients, and one mutation in *ATP6V1B2* gene in two patients (tables 14 and 15). All variants were single-nucleotide substitutions causing missense mutations, with a germline origin, and not annotated in any population database.

KCNH1 and *ATP6V1B2* genes mutations were studied using *in silico* and functional approaches. 3D modeling of KCNH1 and ATP6V1B2 suggest a deleterious effect for the identified mutations, confirming the prediction of *in silico* prediction tools, as Polyphen, SIFT and CADD score. Electrophysiological studies of KCNH1 mutants show that all mutant channels activate to more negative potentials, showing a potential gain-of-function effect.

A following enlargement of the cohort was performed with additional four patients that were analyzed through Sanger sequencing of the coding portion of *KCNH1* and *ATP6V1B2* genes, this screening resulted negative. Two patients were selected for WES leading to the identification of a potentially pathogenic mutation in one patient in the *ATP6V1C1* gene, encoding an interactor of ATP6V1B2.

Common clinical features of patients mutated in *KCNH1*, *ATP6V1B2* and *ATP6V1C1* genes include craniofacial dysmorphism, gingival enlargement, mild to severe intellectual disability, and aplastic or hypoplastic nails and terminal phalanges, although with remarkable variability. Epilepsy was present in all six subjects with *KCNH1* mutations and absent in the patients with *ATP6V1B2* or *ATP6V1C1* mutations. The face is coarser and the hypoplasia of nails and distal phalanges is more severe in patients with mutations in *ATP6V1B2* and *ATP6V1C1*. Other clinical features, such as hearing loss and hypertrichosis, were variably present (table 15).

4.1 *KCNH1*

KCNH1 gene encodes a member of the potassium channel, voltage-gated, subfamily H protein (also called K_v10.1). *KCNH1* is expressed in myoblast at the onset of fusion (Occhiodoro *et al*., 1998) and in adult brain tissue. KCNH1 protein is encoded by two different annotated transcripts (NM_002238, and NM_172362) which differ in the presence of 27 amino acids (aa 318–344) between the transmembrane helices 3 and 4 and encoding the same domains: the amino-terminal region, containing an eag (ether à go-go) domain, the carboxy-terminal region, containing a cyclic nucleotide binding homology domain (CNBHD), and 6 transmembrane helices (S1-S6). The S4 helix works as a voltage sensor domain, the S5 and S6 helices are connected by the P-loop and together constitute the pore. Both the N- and the C-terminal domains are cytoplasmic and are necessary for the gating of the channel (Haitin *et al*., 2013) (figure 21).

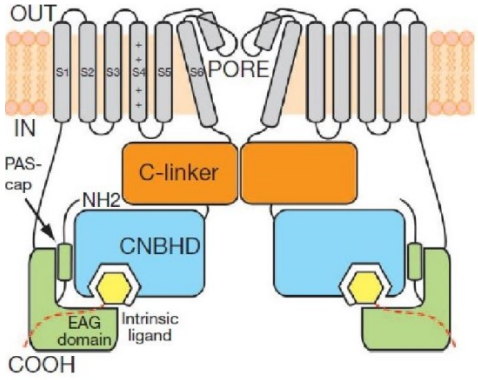

Figure 21. Structure of the eag domain–CNBHD complex of mEAG1 (murine Kcnh1). Cartoon of a cross section of a KCNH channel. Transmembrane domains are in grey, the N-terminal eag domains are in green, the C-linkers are in orange and the CNBHD domains are in blue. The intrinsic ligand motifs are highlighted in yellow, and the post-CNBHD in red (Haitin *et al*., 2013).

The functional channel is a homo- or heterotetramer. During *KCNH1* sequencing analysis we found an alternative isoform expressed in fibroblasts and confirmed also in fetal and adult human brain. This isoform lacks exon 6, encoding the first three transmembrane alpha-helices. A

recent study, demonstrated the presence of short splice variants of KCNH1 resulting from different exon-skipping events in human brain and cancer cell lines (Ramos Gomes *et al*., 2015). Those isoforms lacked the transmembrane domains of the channel and produced cytoplasmic proteins without channel function, that exert their functions inducing a reduction in the overall expression of full-length KCNH1 or affecting its glycosylation pattern. One of these isoforms triggered the activation of cyclin-dependent kinases in *Xenopus laevis* oocytes, suggesting a role in cell cycle control (Ramos Gomes *et al*., 2015). These results highlight the relevance of non-canonical functions of the ion channel KCNH1, whose perturbation could underlie developmental processes.

Gene expression and biochemical studies are ongoing to better characterize this isoform in terms of expression, localization and function, both in patients and in wild-type cells.

Overall, we found 6 *de novo* missense variants in *KCNH1* in six patients c.1054C>G, p.L352V; c.1405G>A, p.G469R; c.1399A>G, p.I467V; c.[974C>A;1066G>C], p.[S325Y;V356L]; and c.1042G>A, p.G348R through exome sequencing and Sanger sequencing screening. Mutation c.1399A>G, p.I467V was found in two patients (cases 4 and 7) (table 14, figure 11).

Most mutations (p.L352V, p.G469R, p.I467V, p. V356L, and p.G348R), involve the helices forming pore (S5 and S6), and S325Y maps into the voltage-sensor helix (S4) (figure 11), suggesting that the ion conductance perturbation could underlie the pathogenic mechanism.

3D modeling studies were performed on 4 of the 6 variants in *KCNH1* (p.L352V, p.V356L, p.I467V, p.G469R). Mutations affecting the residues L352, V356 and I467 impair the closed/open transition of the channel, while the change p.G469R affects the flow of the ions through the pore (figure 12).These results suggest that the molecular size and charge changes of the channel pore could affect the proper functioning of the gate.

Patch-clamp experiments on CHO cells expressing wild-type or mutant KCNH1 channels demonstrated that p.G348R, p.L352V, p.I467V and p.[S325Y; V356L] substitutions have a gain-of-function effect, while the G469R mutant failed to produce voltage-dependent outward currents suggesting that the G469 residue is essential for proper channel gating (figure 13). Experiments in *Xenopus laevis* oocytes documented a dominant action of the G469R mutant over the wild-type channel, with reduced K^+ conductance of the heterotetrameric channels at depolarizing potentials but with pronounced conductance at negative potentials, similar to the other ZLS-causing KCNH1 mutants. Together, these data show a gain-of-function effect for all disease-associated KCNH1 mutants.

In humans, KCNH channels contribute to neuronal signaling in the nervous system and are important regulators of cellular excitability. They have been associated with cancer (Pardo *et al*., 1999), cardiac long QT syndrome type, epilepsy and schizophrenia (Haitin *et al*., 2013). KCNH1

can also be involved in adipogenic and osteogenic differentiation in bone marrow-derived mesenchymal stem cells (Zhang *et al*., 2014). Overexpression of the gene may confer a growth advantage to cancer cells and favor tumor cell proliferation (Ouadid-Ahidouch *et al*., 2016).

KCNH1 plays an active role in cell cycle progression in both cancer and non-transformed cells. Its transcription is directly regulated by the pRb/E2F1 pathway during G2/M, resulting in transient expression that contributes to progression through G2/M. In HeLa cells, KCNH1 depletion leads to delayed G2/M progression, indicating that channel expression at the end of the cell cycle facilitates G2/M completion (Urrego *et al*., 2016)

As recently reported, KCNH1 is a regulator of ciliogenesis (Sánchez *et al*., 2016). The cilium is used as an antennae by the cells to sense the surrounding environment and can be found in cells that are not actively proliferating (Sánchez *et al*., 2016). Experimental evidences demonstrated that KCNH1 localizes to the centrosome and the primary cilium and promotes ciliary disassembly.

This shed light on the role of KCNH1 in the modulation of ciliogenesis, and could potentially explain the influence of KCNH1 expression on the proliferation of normal cells and its tumorigenic effects. Interestingly, a mutant form of KCNH1 was studied, corresponding to mutation L352V found in our case 1 (Sanchez *et al*., 2016). The mutant form of the channel was transfected into wild-type mouse embryonic fibroblasts (MEFs) and its effect on ciliary resorption was tested, demonstrating a significant reduction of ciliated cells (Sanchez *et al*., 2016).

As mutations in KCNH1 show hyperactive effects, this may disrupt cell proliferation and neuronal activity. It could be hypothesized that if KCNH1 is implicated in ciliary resorption, a developmental phenotype in the presence of channel hyperactivity could be related to impaired ciliogenesis.

Interestingly, while mouse model lacking functional Kcnh1 channels appeared normal in their development and in brain morphology, although with mild hyperactivity (Ufartes *et al*., 2013), a recently knockdown model of Kcnh1 in zebrafish delays neural development and causes embryonic lethality, suggesting that Kcnh1 is involved in cell proliferation during early development and that it exerts basic functions beyond neural signaling (Stengel *et al*., 2012).

Recently, *de novo KCNH1* mutations have been reported as disease causing in individuals with Temple-Baraitser syndrome (TMBTS) (Simons *et al*., 2015; Mégarbané *et al*., 2016), a rare developmental disorder characterized by severe mental retardation and anomalies of the hands and feet with absence/hypoplasia of the nails. Most patients have seizures and dysmorphic facial features (Jacquinet *et al*., 2010). All nine reported TMBTS-affected individuals presented with absent or hypoplastic thumb and great toenails, and epileptic seizures with varying age of onset, but none of them was described to have gingival hyperplasia (Simons *et al*., 2015; Mégarbané *et al*.,

2016). Functional studies in two different cell systems demonstrated that the TMBTS-associated *KCNH1* mutations were gain-of-function mutations, lowering the activation threshold of the mutant KCNH1 channels and delaying their deactivation (Simons *et al*. 2015). This syndrome has many overlaps with ZLS in terms of orofacial and digital abnormalities, and epilepsy.

More recently, further patients with *KCNH1* mutations have been reported with intellectual disability (Bramswig *et al*., 2015), and a phenotype characterized by syndromic developmental delay, hypotonia and seizures (Fukai *et al*., 2016).

So far a total of 21 individuals with pathogenic *KCNH1* variants have been published (Kortum *et al*., 2015; Simons *et al*., 2015; Bramswig *et al*., 2015; Fukai *et al*., 2016; Mégarbané *et al*., 2016). These patients carry 12 different *KCNH1* mutations, suggesting the presence of mutation hot spots corresponding to the S4–S6 domains and highlighting the functional importance of those domains in KCNH1 (figure 22). These findings indicate that there is no correlation between the location of the affected residues and the clinical diagnosis.

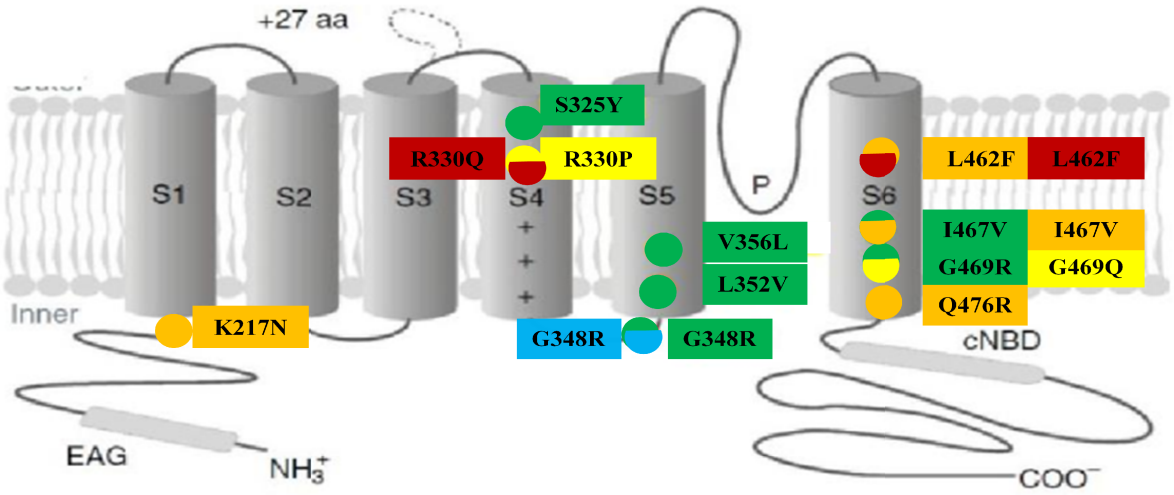

Figure 22. Schematic representation of all the mutations found in *KCNH1*. In green the mutations reported in this work, in orange mutations reported in Simons *et al*., 2015, in red mutations reported in Bramswig *et al*., 2015, in yellow mutations reported in Fukai *et al*., 2016, and in blue the mutation reported in Mégarbané *et al*., 2016.

Moreover, in at least five cases, the same mutation has been reported in association with different clinical diagnosis (c.1399A>F, p.I467V associated with ZLS and TMBTS, Kortum *et al*., 2015; Simons *et al*., 2015). Patients share some features like intellectual disability, seizures, coarse face, and hypoplastic nails and terminal phalanges. However, they also show different clinical features, e.g. with regard to their development and onset of epilepsy, deafness, gingival hyperplasia, and hirsutism (table 19).

Thus, there might be other factors involved, i.e. genetic modifiers, that prevent the prediction of some features, e.g. occurrence and age of onset of epileptic seizures, from the presence and the location of a pathogenic KCNH1 mutation.

Mutation	c.1399A>G p.I467V					
Reference	Present work (Kortum *et al.*, 2015)		Simons *et al.*, 2015			Total
Case	4	7	3	5	6	5
Diagnosis	ZLS		TMBTS			
Sex	F	F	M	F	F	1M:4F
ID	+	+	+	NR	+	4/4
Seizures	+	+	+	+	+	5/5
Hypotonia	+	-	+	+	+	4/5
Deafness	-	+	-	-	-	1/5
Coarse Face	+	+	+	+	+	5/5
Gingival hyperplasia	+	-	-	-	-	1/5
Hypoplastic Nails	+	+	+	+	+	5/5
Hypoplastic phalanges	+	+	+	+	+	5/5
Scoliosis	+	NR	NR	NR	NR	1/1
Hirsutism	+	-	-	-	-	1/5

Table 19. Clinical features of the patients carrying the same mutation in *KCNH1* reported in literature.
M = male, F = female, + = present, - = absent, ID = Intellectual disability, NR = not reported, ZLS = Zimmermann-Laband syndrome, TMBTS = Temple-Baraitser syndrome.

A comparison of clinical features of all *KCNH1* mutated patients to date reported in literature, allowed us to disclose the presence of some features shared among patients, like severe intellectual disability, neonatal hypotonia, seizures of varying age of onset, and hypoplastic nails.

Even though gingival hyperplasia has not been reported in TMBTS-affected individuals (Simons *et al*. 2015), is a frequent clinical feature in individuals with *KCNH1* mutations. The limb phenotype is variable and may include the absence/hypoplasia of the thumb nails, hallux nails, and other finger-/toenails. In addition, the thumbs can be long and proximally implanted. Deafness and hirsutism are observed in only a small fraction of the cases. The main clinical features of the *KCNH1* mutated patients are summarized in table 20.

	Present Work, Kortum *et al.*, 2015	Simons *et al.*, 2015	Bramswig *et al.*, 2015	Fukai *et al.*, 2016	Mégarbané *et al.*, 2016	Total
N. of cases	6	6	4	4	1	21
Diagnosis	ZLS	TMBTS	ID	SDDHS	TMBTS	
Sex	2M:4F	2M:4F	4F	4M	M	9M:12F
ID	6/6	5/5	4/4	4/4	+	20/20
Seizures	6/6	6/6	3/4	4/4	-	19/21
Hypotonia	4/6	6/6	4/4	3/4	+	18/21
Deafness	1/4	0/6	0/4	0/4	-	1/19
Coarse Face	6/6	6/6	4/4	3/4	+	20/21
Gingival hyperplasia	5/6	0/6	4/4	1/4	+	11/21
Hypoplastic Nails	5/6	6/6	4/4	3/4	+	19/21
Hypoplastic phalanges	4/5	5/6	0/4	0/4	-	9/20
Scoliosis	5/6	NR	NR	0/4	NR	5/10
Hirsutism	3/6	0/6	0/4	0/4	-	3/21

Table 20. A summary of the main ZLS features is presented and compared with clinical features of other *KCNH1* mutated patients. M=male, F=female, +=present, -=absent, ID=Intellectual disability, NR=not reported, ZLS=Zimmermann-Laband syndrome, TMBTS=Temple-Baraitser syndrome, SDDHS=Syndromic Developmental Delay, Hypotonia and Seizures.

Therefore, we can conclude that there is not a clear genotype-phenotype correlation among *KCNH1* mutations and clinical features and that the mutations in *KCNH1* likely cause a phenotypic *continuum* of neurodevelopmental disorders covering both ZLS and TMBTS.

More information of *KCNH1* mutations and their clinical consequences are needed, in order to more clearly delineate the genotype-phenotype correlation, and to characterize the molecular mechanisms involved in the pathogenesis of this phenotypic spectrum.

In one patient (case 5) we found two de *novo* mutations in *KCNH1* on the same allele (c.[974C>A;1066G>C]; p.[S325Y;V356L]), 92 nucleotides apart (figure 9). This is a very unusual occurrence. Multiple mutations that exhibit nonrandom proximal spacing in higher eukaryotes are termed ‘‘closely spaced multiple mutations’’ (CSMMs) and are most compatible with a model in which they are generated simultaneously or *quasi*-simultaneously in the same cell cycle (Colgin *et al.*, 2002; Hill *et al.*, 2004). Examples of pathogenic CSMMs are known from a collection of human inherited disease-causing multiple mutations (Chen *et al.*, 2009). Two single-base substitutions (C>G and T>C) separated by 25 bp, causing two different *cis* amino acid substitutions in the androgen receptor gene on the maternal X-chromosome have been reported in feminized, male monozygotic twins (Mongan *et al.*, 2002). A patient with Multiple Endocrine Neoplasia, type IIA

(MEN2A) have been reported to have two *cis* missense substitutions in the *RET* gene resulting from single base substitutions (C>T and C>G) separated by 19 bp (Tessitore *et al*., 1999). An additional case with two single-base changes separated by nine nucleotides in the *ELA2* gene, predicting two amino acid substitutions (p.V69L and p.V72L), is reported (Salipante *et al*., 2007).

Multiple synchronous mutations have been postulated to arise via transient hypermutability, resulting from the deregulated expression of a replicative DNA polymerase or another protein involved in the maintenance of replication fidelity, the disruption of the balance of the nucleotide pool, or the recruitment of error-prone polymerases (Chen *et al*., 2009). The onset of CSMMs has been studied in mouse models or in human cell lines, but the actual mechanisms that cause them is not yet clear.

One of the two changes, p.S325Y, is predicted as "pathogenic" by Polyphen, SIFT and CADD score, while the other, p.V356L, is predicted as "benign" by Polyphen and SIFT. Moreover, they map in residues that are both less conserved than the other *KCNH1* mutated residues (figure 10).

4.2 *ATP6V1B2*

ATP6V1B2 encodes one of two V_1 domain B subunit isoforms of the V-ATPase proton pump and is the only B isoform highly expressed in osteoclasts. V-ATPase dependent organelle acidification is necessary for intracellular processes such as protein sorting, zymogen activation, receptor-mediated endocytosis, and synaptic vesicle proton gradient generation. V-ATPase is composed of a cytosolic V_1 domain and a transmembrane V_0 domain. The V_1 domain consists of three A, three B, and two G subunits, as well as a C, D, E, F, and H subunit. The V_1 domain contains the ATP catalytic site.

We found one *de novo* variant in *ATP6V1B2* in two ZLS patients, c.1454G>C (p.R485P), through exome sequencing. 3D modeling studies predicted that the substitution of the R485 with a proline perturb intersubunit interactions within the V_1 subcomplex, possibly preventing the formation of a functional V-ATPase. Clinical features of cases 2 and 8 include gingival enlargement, anonychia of the hands and feet, aplastic terminal phalanges of the fingers and toes, and hypertrichosis (table 21).

Recently, a heterozygous truncating *ATP6V1B2* mutation, c.1516C>T (p.R506*), has been reported in three patients with autosomanl dominant deafness and onychoystrophy syndrome (DDOD) (Yuan *et al*., 2014). DDOD patients mutated in *ATP6V1B2* show hypoplasia of nails and terminal phalanges but no intellectual disability, coarse face, gingival hyperplasia, or hirsutism (figure 23 and table 21). Among all the *ATP6V1B2* mutated patients, deafness is present in all the

three DDOD cases but only in one patient analyzed in the present work (table 21). The DDOD mutation inserts a premature stop codon that prevents the synthesis of the last six amino acids. Cell studies demonstrated that the truncated protein reduced the ATP hydrolysis mediated by the V-ATPase and also the acidification of the intracellular organelles. In figure 24 the positions of the mutated residues with respect to the assembled V-ATPase are represented.

Consistent with partial clinical overlap, the ZLS- and DDOD-causing mutations in *ATP6V1B2* affect the same protein region, which participates in V_1 subcomplex assembly. These mutations can both lead to a reduction of the number of functional V-ATPases. Functional studies are required to understand the consequences of these alterations on the proper assembly/function of the V-ATPase.

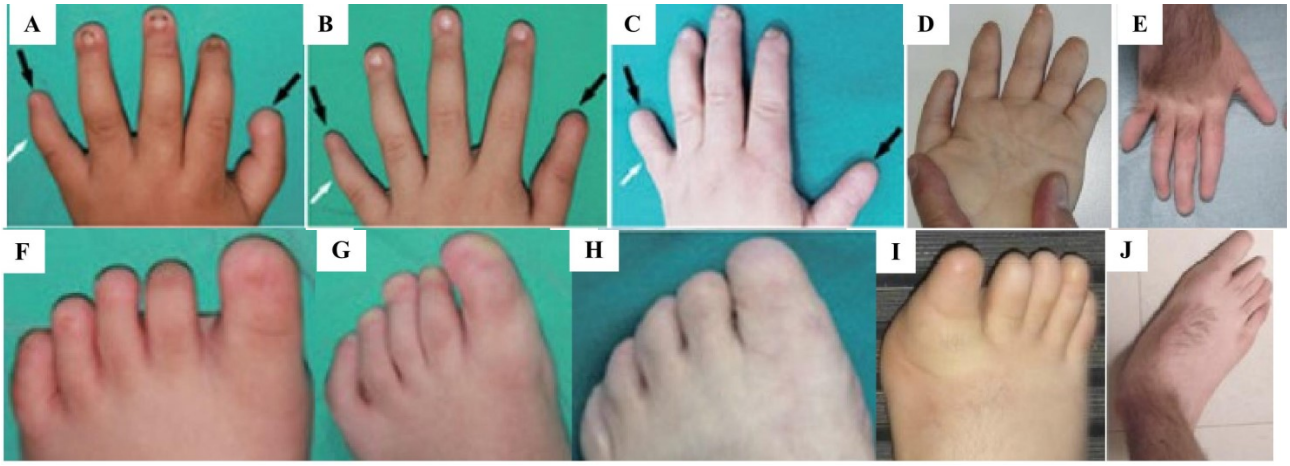

Figure 23. (A-C, F-H) Hands and feet of three patients with DDOD, mutated in *ATP6V1B2* (Yuan *et al*., 2014), **(D,E,I,J)** Hands and feet of cases 7 and 8 of the present work, mutated in *ATP6V1B2* (Kortum *et al*., 2015). **(A-C)** Pictures of the hands of the DDOD patients showing the absence of the fifth finger and thumb nails indicated by black arrows, aplasia of the middle phalanx in the fifth fingers indicated by white arrows, hypoplasia of the middle three fingernails. **(F-G)** Pictures of the feet of the DDOD patients showing the absence of all toenails. **(D,E,I,J)** Hands and feet of cases 7 and 8 with ZLS showing nails and phalanges aplasia. (**D,I**) Case 7 shows shortened second to fourth fingers, except the third finger on the right hand, and toes. Case 8 shows aplastic terminal phalanges of the fifth finger on the right hand and all toes except the first.

Mutation	c.1454G>C p.R485P		c.1516C>T p.R506*		
Reference	Present work (Kortum *et al.*, 2015)		Yuan *et al.*, 2014		
Case	2	8	1	2	3
Diagnosis	ZLS		DDOD		
Sex	F	M	F	M	F
ID	+	+	-	-	-
Seizures	-	-	-	-	-
Hypotonia	+	+	-	-	-
Deafness	-	+	+	+	+
Coarse face	+	+	-	-	-
Gingival hyperplasia	+	+	-	-	-
Hypoplastic nails	+	+	+	+	+
Hypoplastic phalanges	+	+	+	+	+
Scoliosis	-	+	NR	NR	NR
Hirsutism	+	+	-	-	-

Table 21. A summary of the main clinical feature of *ATP6V1B2* mutated patients.
M = male, F = female, + = present, - = absent, NR = not reported, ZLS = Zimmermann-Laband syndrome, DDOD = Dominant deafness onychodystrophy syndrome.

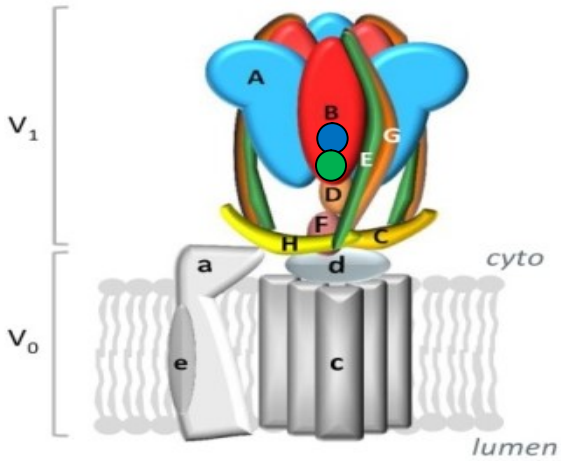

Figure 24. Schematic view of the subunit structure of the V-ATPase. The catalytic V_1 complex consists of the A, B, C, D, E, F, G and H subunits. The V_0 domain is membrane embedded and is composed of a characteristic C-ring structure with which the a, d and e subunits are associated. The blue dot indicate the R485 residue, the green dot represent the R506 residue.

4.3 *ATP6V1C1*

ATP6V1C1 encodes the subunit C, that constitutes the V_1 subcomplex of the V-ATPase proton pump. The subunit C, together with the subunits E, G, and H, and the N-terminal domain of

subunit a, make up the peripheral stalks and serve to tether V_1 to V_0 subcomplexes (Cotter *et al*., 2015). ATP6V1C1 has also a regulatory role in the V-ATPase assembly. It can trigger the formation of functional proton pumps in response to various stimuli, like increasing of glucose level, activation of PI3K, mTORC1 and EGF pathways (Cotter *et al*., 2015).

ATP6V1C1 is expressed in activated osteoclasts when these cells operate bone reabsorption (Feng *et al*., 2009). ATP6V1C1 can also bind G-actin, increasing its polymerization rate, stabilization and crosslinking F-actin (Vitavska *et al*., 2003, Vitavaska *et al*., 2005). Another important function is its role in cellular proliferation, it is indeed overexpressed in several type of cancers like oral squamous carcinoma and breast cancer (Feng *et al*., 2014).

By WES approach we found a *de novo* mutation in *ATP6V1C1*, c.865G>A (p.E289K) in one ZLS patient. This patient (case 9) shows remarkably overlapping features with ATP6V1B2 mutated patients analyzed in the present work. Those patients share a coarse face, intellectual disability, and hypoplastic nails and phalanges, although *ATP6V1C1* mutated individual lacks gingival hyperplasia and hirsutism (table 22).

ATP6V1B2 and ATP6V1C1 constitute the V_1 subcomplex, ATP6V1B2-econded subunit constitutes the ATPase domain together with the A subunits, while the C subunit constitutes the stalk that link A-B subunits to the V_o subcomplex. On the basis of the phenotypic similarity among *ATP6V1B2*- and *ATP6V1C1*-mutated patients and the structural analysis of ATP6V1B2 mutant protein, it can be hypothesized that the p.E289K mutation of ATP6V1C1 could exert a similar effect, impairing the biogenesis of a functional V-ATPase. Structural and functional studies are ongoing to characterize the effect of the p.E289K mutation on the proper assembly/activity of the ATPase complex.

Gene	*ATP6V1B2*		*ATP6V1C1*
Mutation	c.1454G>C p.R485P		c.865G>A p.E289K
Case	2	8	9
Sex	F	M	F
ID	+	+	+
Seizures	-	-	-
Deafness	-	+	+
Coarse face	+	+	+
Gingival hyperplasia	+	+	-
Hypoplastic nails	+	+	+
Hypoplastic phalanges	+	+	+
Scoliosis	-	+	NR
Hirsutism	+	+	-

Table 22. A comparison of the main clinical features of patients *ATP6V1B2* and *ATP6V1C1* mutated respectively. M=male, F=female, +=present, -=absent, NR=not reported.

The mosaicism for the *ATP6V1C1* variant allele in the father's proband fitted with a mild manifestation of some ZLS features also in this subject.

Standard workflow analyses of WES data were not able to detect the presence of the pathogenic allele in the father's blood cells, as the algorithm used to disclose the presence of DNA mutations discards reads in low percentage, as they potentially represent sequencing and/or alignment errors. When a different pipeline (MuTect2, Cibulskis *et al*., 2013), specifically designed to disclose the presence of low percentage variant allele, was used, we were able to identify the mutation also in the mildly affected father (figures 16 and 19). This suggests that using bioinformatic tools that usually identify somatic mutations in tumoral samples, can be useful also for Mendelian diseases.

These results confirmed the role of mosaicism in Mendelian diseases, causing a milder phenotype than when present in the germline. Recent technological advances in genomics have enhanced the ability to detect and characterize different types of mosaicism with increasing sensitivity, demonstrating the widespread nature of mosaicism in a wide range of disorders.

Although the accurate differentiation between sequencing error and a mosaic mutation is a challenging task, mosaicism levels as low as 2% could be distinguished from sequencing errors using dedicated analysis tools. Mosaic disorders pose a new challenge for genotype-phenotype correlations and prediction of disease manifestations and severity, with several clinical implications, in terms of recurrence risk and prognosis.

4.4 *ATP6V1B2* and *ATP6V1C1*: the role of V-ATPase

The eukaryotic V-type ATPase (V-ATPase) is a multi-subunit membrane protein complex that has an important role in both endocytosis and intracellular transport. In receptor-mediated endocytosis, a low pH within early endosomes triggers the dissociation of internalized ligand–receptor complexes. This allows for recycling of receptors to the plasma membrane, V-ATPases located in the apical membrane of type-A renal intercalated cells function in proton secretion into the renal fluid and hence in acid–base balance in the kidney, in macrophages and neutrophils.

Plasma membrane V-ATPases also have an important role in bone resorption. Osteoclasts attach to the surface of bone to create a sealed extracellular compartment, acidification of this space serves to both dissolve the bone matrix and to increase the activity of acid hydrolases that are secreted by the osteoclast (Nishi and Forgac, 2002).

Several pathways have been identified (e.g. mTOR pathway, WNT signal transduction pathway, Notch pathway) involving V-ATPase functions (Sun-Wada and Wada 2015), highlighting its crucial role in cell pathways whose dysregulation could underlie ZLS pathogenesis. To date, there are no clear links between V-ATPase cell functions and pathogenic mechanisms underlying ZLS phenotype. The identification of a further mutated subunit in a ZLS patient and the clinical overlap of *ATP6V1B2* and *ATP6V1C1* mutated patients suggests that V-ATPase have a significant role in developmental processes, yet to be identified, whose dysregulation could determine several developmental defects.

4.5 Mutations in *ATP6V1B2*, *ATP6V1C1*, and *KCNH1*: the question of splitting or lumping

We identified *KCNH1*, *ATP6V1B2*, and *ATP6V1C1* as disease-associated genes for ZLS. So far, only hypothetical functional links exist between *KCNH1*, and *ATP6V1B2* and *ATP6V1C1*. Both the V-ATPase and KCNH1 have been shown to regulate neurotransmitter release and are important for synaptic transmission (Mortensen *et al*., 2014; Poëa-Guyon *et al*., 2013). The V-ATPase, as already stated, serves in the acidification of intracellular organelles, and effective proton pumping requires the movement of a counterion. Initial data indicate that K^+ could act as the counterion (Steinberg *et al*., 2010). Rapid internalization of plasma membrane–localized KCNH1 and its sorting to lysosomes provide a first clue of the function of KCNH1 in lysosomal conductive pathways. Alternatively, altered acidification of intracellular compartments may lead to disturbances in cellular transport processes in general and to perturbed regulation of KCNH1 trafficking in particular (Kohl *et al*., 2011).

A comparison of phenotypes associated with mutations in KCNH1 and ATPase subunits suggests that ATPase subunits mutations cause a more pronounced phenotype characterized mostly by hypertrichosis, limb anomalies (including aplastic terminal phalanges and anonychia of hands and feet), and a coarser facial phenotype. These results suggest that there is a clinical overlap but probably they represent distinct phenotypes.

The original and following published patients with a clinical diagnosis of ZLS also show coarse facial features, a large nose which can be poorly formed due to soft cartilage and hypoplastic terminal phalanges (Bazopoulou-Kyrkanidou *et al*. 1990; Laband *et al*. 1964). Taken together, all these results led us to hypothesize that the ZLS patients with *KCNH1* mutations belong to the TMBTS spectrum, while the individuals with *ATP6V1B2* and *ATP6V1C1* mutations represent the original and more severe ZLS spectrum. This led to a debate, about the "splitting" or "lumping" approach to study these disorders (Bramswig *et al*., 2015), that is still ongoing.

However, due to the limited number of individuals described, some with only scarce clinical data and no clinical photographs, it is difficult to draw an accurate conclusion. Additional patients with a TMBTS/ZLS phenotype are needed to further investigate this phenotypic spectrum and give some hints to come to a final conclusion about the above-mentioned hypotheses. It would be insightful also to perform a detailed characterization of the molecular bases of these disorders, in order to understand the mechanisms by which these genes cause the pathogenesis of these syndromes.

Moreover, the presence of several ZLS patients (Kortum *et al*., 2015 and the present work) mutation negative for *KCNH1*, *ATP6V1B2*, and *ATP6V1C1* suggests further genetic heterogeneity.

To this aim, we are currently recruiting patients with ZLS and ZLS-like phenotype. Patients will be screened by Sanger sequencing of the coding portions of *KCNH1*, *ATP6V1B2*, *ATP6V1C1* genes. Mutation positive patients will be analyzed in order to provide a more accurate picture of the molecular spectrum of mutations and their associated clinical spectrum. Patients that will be found mutation negative will be considered for WES/WGS-based approaches directed to identify the missing disease genes.

Functional studies are ongoing in order to better characterize the altered function of the mutated genes and the perturbed pathways that cause the pathogenic mechanism.

5. Conclusions

Zimmermann-Laband syndrome is a rare developmental disorder characterized by facial dysmorphism, nail aplasia or hypoplasia, hypertrichosis, and intellectual disability with or without epilepsy. In this work (Kortum *et al*., 2015) we identified for the first time the causative genes that highlight the role of potassium channels (*KCNH1*) and the vacuolar ATPase (*ATP6V1B2* and *ATP6V1C1*) in the pathogenesis of this disorder.

The identification of two genes (*KCNH1* and *ATP6V1B2*) involved also in clinically overlapping phenotypes (Temple-Baraitser syndrome, intellectual disability, syndromic developmental delay, hypotonia and seizures and dominant deafness and onychodystrophy syndrome), suggest that they cause a phenotypic spectrum. These observations allowed to conclude that the characterization of the molecular bases of these overlapping syndromes could represents a powerful tool for their classification.

Genetic evidence points to a genetically heterogeneity for ZLS, indicating that additional unknown genes are involved. An enlargement of the cohort of patients would provide additional data to perform genotype-phenotype correlations and further characterize the genetic heterogeneity of this syndrome.

Our understanding of the molecular events underlying this condition will provide new tools for diagnosis of this rare disorder, with direct impact on diagnosis, prognosis, counseling, and patient management.

6. Websites

1- http://www.1000genomes.org/
2- http://evs.gs.washington.edu/EVS/
3- http://exac.broadinstitute.org/
4- http://geneontology.org/
5- https://www.genome.ucsc.edu/
6- https://www.ncbi.nlm.nih.gov/genbank/
7- https://www.ncbi.nlm.nih.gov/homologene
8- https://www.ncbi.nlm.nih.gov/snp
9- https://omim.org/
10- http://www.uniprot.org/

7. References

1- Abo-Dalo, B., Kim, H.G., Roes, M., Stefanova, M., Higgins, A., Shen, Y., Mundlos, S., Quade, B.J., Gusella, J.F., and Kutsche, K. (2007). Extensive molecular genetic analysis of the 3p14.3 region in patients with Zimmermann-Laband syndrome. Am. J. Med. Genet. A. *143A*(22):2668-2674.

2- Abo-Dalo, B., Roes, M., Canún, S., Delatycki, M., Gillessen-Kaesbach, G., Hrytsiuk, I., Jung, C., Kerr, B., Mowat, D., Seemanova, E., Steiner, C.E., Stewart, H., Thierry, P., van Buggenhout, G., White, S., Zenker, M., and Kutsche, K. (2008). No mutation in genes of the WNT signaling pathway in patients with Zimmermann-Laband syndrome. Clin. Dysmorphol. *17*(3):181-185.

3- Adzhubei, I.A., Schmidt, S., Peshkin, L., Ramensky, V.E., Gerasimova, A., Bork, P., Kondrashov, A.S., and Sunyaev, S.R. (2010). Nat. Methods. *7*(4):248-249.

4- Alavandar, G. (1965). Elephantiasis gingivae. Report of an affected family with associated hepatomegaly, soft tissue and skeletal abnormalities. J. All. India Dent. Assoc. *37*

5- Atabek, M.E., Pirgon, O., Sert, A., and Toy, H. (2005). Zimmermann-Laband syndrome in an infant with an atypical histological finding. Pediatr. Dev. Pathol. *8*(6):654-657.

6- Azaiez, H., Booth, K.T., Bu, F., Huygen, P., Shibata, S.B., Shearer, A.E., Kolbe, D., Meyer, N., Black-Ziegelbein, E.A., and Smith, R.J. (2014). *TBC1D24* mutation causes autosomal-dominant nonsyndromic hearing loss. Hum. Mutat. *35*(7):819-823.

7- Bakaeen, G., and Scully, C. (1991). Hereditary gingival fibromatosis in a family with the Zimmermann-Laband syndrome. J. Oral. Pathol. Med. *20*(9):457-459.

8- Balasubramanian, M., and Parker, M.J. (2010). Zimmermann-Laband syndrome in a child previously described with brachydactyly, extrahepatic biliary atresia, patent ductus arteriosus and seizures. Clin. Dysmorphol. *19*(1):48-50.

9- Bramswig, N.C., Ockeloen, C.W., Czeschik, J.C., van Essen, A.J., Pfundt, R., Smeitink, J., Poll-The, B.T., Engels, H., Strom, T.M., Wieczorek, D., Kleefstra, T., and Lüdecke, H.J. (2015). 'Splitting versus lumping': Temple-Baraitser and Zimmermann-Laband Syndromes. Hum. Genet. *134*(10):1089-1097.

10- Campeau, P.M., Kasperaviciute, D., Lu, J.T., Burrage, L.C., Kim, C., Hori, M., Powell, B.R., Stewart, F., Félix, T.M., van den Ende, J., Wisniewska, M., Kayserili, H., Rump, P., Nampoothiri, S., Aftimos, S., Mey, A., Nair, L.D., Begleiter, M.L., De Bie, I., Meenakshi, G., Murray, M.L., Repetto, G.M., Golabi, M., Blair, E., Male, A., Giuliano, F., Kariminejad, A., Newman, W.G., Bhaskar, S.S., Dickerson, J.E., Kerr, B., Banka, S., Giltay, J.C., Wieczorek, D., Tostevin, A., Wiszniewska, J., Cheung, S.W., Hennekam, R.C., Gibbs, R.A., Lee, B.H., and Sisodiya, S.M. (2014). The genetic basis of DOORS syndrome: an exome-sequencing study. Lancet Neurol. *13*(1):44-58.

11- Castori, M., Valiante, M., Pascolini, G., Leuzzi, V., Pizzuti, A., and Grammatico, P. (2013). Clinical and genetic study of two patients with Zimmermann-Laband syndrome and literature review. Europ. J. Med. Genet. *56*:570-576.

12- Chacon-Camacho, O.F., Vázquez, J., and Zenteno, J.C. (2011). Expanding the phenotype of gingival fibromatosis-mental retardation-hypertrichosis (Zimmermann-Laband) syndrome. Am. J. Med. Genet. A. *155A*(7):1716-1720.

13- Chen, J.M., Férec, C., and Cooper, D.N. (2009). Closely spaced multiple mutations as potential signatures of transient hypermutability in human genes. Hum. Mutat. *30*(10):1435-1448.

14- Chodirker, B. N., Chudley, A. E., Toffler, M. A., and Reed, M. H. (1986). Zimmerman-Laband syndrome and profound mental retardation. Am. J. Med. Genet. *25*:543-547.

15- Chun, S., and Fay, J.C. (2009). Identification of deleterious mutations within three human genomes. Genome Res. *19*(9):1553-1561.

16- Cibulskis, K., Lawrence, M.S., Carter, S.L., Sivachenko, A., Jaffe, D., Sougnez, C., Gabriel, S., Meyerson, M., Lander, E.S., and Getz, G. (2013). Sensitive detection of somatic point mutations in impure and heterogeneous cancer samples. Nat. Biotechnol. *31*(3):213-219.

17- Cingolani, P., Platts, A., Wang, l.-L., Coon, M., Nguyen, T., Wang, L., Land, S.J., Lu, X., and Ruden, D.M. (2012). A program for annotating and predicting the effects of single

nucleotide polymorphisms, SnpEff: SNPs in the genome of Drosophila melanogaster strain w1118; iso-2; iso-3. Fly (Austin). *6*(2):80-92.

18- Colgin, L.M., Hackmann, A.F., Emond, M.J., and Monnat, R.J. Jr. (2002). The unexpected landscape of in vivo somatic mutation in a human epithelial cell lineage. Proc. Nat'l Acad. Sci. U.S.A. *99*(3):1437-1442.

19- Cooper, G.M., Stone, E.A., Asimenos, G., NISC Comparative Sequencing Program, Green, E.D., Batzoglou, S., and Sidow, A. (2005). Distribution and intensity of constraint in mammalian genomic sequence. Genome Res. *15*(7):901-913.

20- Cotter, K., Stransky, L., McGuire, C., and Forgac, M. (2015). Recent Insights into the Structure, Regulation, and Function of the V-ATPases. Trends Biochem. Sci. *40*(10):611-622.

21- Davalos, I. P., Garcia-Cruz, D., Garcia-Cruz, M. O., Ramirez-Duenas, M. L., Solis-Camara, P., Correa-Cerro, L. S., Perez-Rulfo, D., and Sanchez-Corona, J. (2005). Zimmermann-Laband syndrome: further clinical delineation. Genet. Counsel. *16*:283-290.

22- Davalos, I. P., Brambila-Tapia, A. J. L., Davalos, N. O., Duran-Gonzalez, J., Gonzalez-Mercado, M. G., Cruz-Ramos, J. A., Rios-Gonzalez, B. E., E'Vega, R., Zavala-Cerna, M. G., Garcia-Cruz, M. O., and Garcia-Cruz, D. (2011). Wide clinical spectrum in Zimmermann-Laband syndrome. Genet. Counsel. *22*:1-10.

23- Davydov, E.V., Goode, D.L., Sirota, M., Cooper, G.M., Sidow, A., and Batzoglou, S. (2010). Identifying a high fraction of the human genome to be under selective constraint using GERP++. PLoS Comput. Biol. *6*(12).

24- Dumić, M., Crawford, C., Ivković, I., Cvitanović, M., and Batinica, S. (1999). Zimmerman-Laband syndrome: An unusually early presentation in a newborn girl. Croat. Med. J. *40*(1):102-103.

25- Felsenstein, J., and Churchill, G. (1996). A hidden Markov model approach to variation among sites in rate of evolution. Mol. Biol. Evol. *13*:93-104.

26- Feng, S., Zhu, G., McConnell, M., Deng, L., Zhao, Q., Wu, M., Zhou, Q., Wang, J., Qi, J., Li, Y.P., and Chen W. (2013). Silencing of atp6v1c1 prevents breast cancer growth and bone metastasis. Int. J. Biol. Sci. *9*(8):853-862.

27- Feng, S., Deng, L., Chen, W., Shao, J., Xu, G., and Li, Y.P. (2009). Atp6v1c1 is an essential component of the osteoclast proton pump and in F-actin ring formation in osteoclasts. Biochem. J. *417*(1):195-203.

28- Fukai, R., Saitsu, H., Tsurusaki, Y., Sakai, Y., Haginoya, K., Takahashi, K., Hubshman, M.W., Okamoto, N., Nakashima, M., Tanaka, F., Miyake, N., and Matsumoto, N. (2016).

De novo KCNH1 mutations in four patients with syndromic developmental delay, hypotonia and seizures. J Hum Genet. *61*(5):381-387.

29- Gabbett, M. T., Clark, R. C., and McGaughran, J. M. (2008). A second case of severe mental retardation and absent nails of hallux and pollex (Temple-Baraitser syndrome). Am. J. Med. Genet. *146A*:450-452.

30- Haitin, Y., Carlson, A.E., and Zagotta, W.N. (2013). The structural mechanism of KCNH-channel regulation by the eag domain. Nature. *501*(7467):444-448.

31- Harakalova, M., van Harssel, J.J., Terhal, P.A., van Lieshout, S., Duran, K., Renkens, I., Amor, D.J., Wilson, L.C., Kirk, E.P., Turner, C.L., Shears, D., Garcia-Minaur, S., Lees, M.M., Ross, A., Venselaar, H., Vriend, G., Takanari, H., Rook, M.B., van der Heyden, M.A., Asselbergs, F.W., Breur, H.M., Swinkels, M.E., Scurr, I.J., Smithson, S.F., Knoers, N.V., van der Smagt, J.J., Nijman, I.J., Kloosterman, W.P., van Haelst, M.M., van Haaften, G., and Cuppen E. (2012). Dominant missense mutations in ABCC9 cause Cantú syndrome. Nat. Genet. *18*;44(7):793-796.

32- Hill, K.A., Wang, J., Farwell, K.D., Scaringe, W.A., and Sommer, S.S. (2004). Spontaneous multiple mutations show both proximal spacing consistent with chronocoordinate events and alterations with p53-deficiency. Mutat. Res. *554*(1-2):223-240.

33- Hoogendijk, C.F., Marx, J., Honey, E.M., Pretorius, E., and Christianson, A.L. (2006). Ultrastructural investigation of Zimmermann-Laband syndrome. Ultrastruct. Pathol. *30*(6):423-426.

34- Holzhausen, M., Gonçalves, D., Corrêa Fde, O., Spolidorio, L.C., Rodrigues, V.C., and Orrico, S.R. (2003). A case of Zimmermann-Laband syndrome with supernumerary teeth. J. Periodontol. *74*(8):1225-1230.

35- Jacquinet, A., Gerard, M., Gabbett, M. T., Rausin, L., Misson, J.-P., Menten, B., Mortier, G., Van Maldergem, L., Verloes, A., and Debray, F.-G. (2010). Temple-Baraitser syndrome: a rare and possibly unrecognized condition. Am. J. Med. Genet. *152A*:2322-2326.

36- Kim, H.G., Higgins, A.W., Herrick, S.R., Kishikawa, S., Nicholson, L., Kutsche, K., Ligon, A.H., Harris, D.J., MacDonald, M.E., Bruns, G.A., Morton, C.C., Quade, B.J., and Gusella, J.F. (2007). Candidate loci for Zimmermann-Laband syndrome at 3p14.3. Am. J. Med. Genet. A. *143A*(2):107-111.

37- Kircher, M., Witten, D.M., Jain, P., O'Roak, B.J., Cooper, G.M., and Shendure, J. (2014). A general framework for estimating the relative pathogenicity of human genetic variants. Nat. Genet.

38- Koch, P., Wettstein, A., Knauber, J., and Zaun, H. (1992). A new case of Zimmermann-Laband syndrome with atypical retinitis pigmentosa. Acta Derm. Venereol. *72*:376-379.

39- Kohl, T., Lörinczi, E., Pardo, L.A., and Stühmer, W. (2011). Rapid internalization of the oncogenic K+ channel K(V)10.1. PLoS One. *6*(10):e26329.

40- Kortüm, F., Caputo, V., Bauer, C.K., Stella, L., Ciolfi, A., Alawi, M., Bocchinfuso, G., Flex, E., Paolacci, S., Dentici, M.L., Grammatico, P., Korenke, G.C., Leuzzi, V., Mowat, D., Nair, L.D., Nguyen, T.T., Thierry, P., White, S.M., Dallapiccola, B., Pizzuti, A., Campeau, P.M., Tartaglia, M., and Kutsche, K. (2015). Mutations in KCNH1 and ATP6V1B2 cause Zimmermann-Laband syndrome. Nat. Genet. *47*(6):661-667.

41- Kumar, P., Henikoff, S., and Ng, P.C. (2009). Predicting the effects of coding non-synonymous variants on protein function using the SIFT algorithm. Nat. Protoc. *4*(7):1073-1081.

42- Laband, P. F., Habib, G., and Humphreys, G. S. (1964). Hereditary gingival fibromatosis: report of an affected family with associated splenomegaly and skeletal and soft-tissue abnormalities. Oral. Surg. *17*:339-351.

43- Lek, M., Karczewski, K.J., Minikel, E.V., Samocha, K.E., Banks, E., Fennell, T., O'Donnell-Luria, A.H., Ware, J.S., Hill, A.J., Cummings, B.B., Tukiainen, T., Birnbaum, D.P., Kosmicki, J.A., Duncan, L.E., Estrada, K., Zhao, F., Zou, J., Pierce-Hoffman, E., Berghout, J., Cooper, D.N., Deflaux, N., DePristo, M., Do, R., Flannick, J., Fromer, M., Gauthier, L., Goldstein, J., Gupta, N., Howrigan, D., Kiezun, A., Kurki, M.I., Moonshine, A.L., Natarajan, P., Orozco, L., Peloso, G.M., Poplin, R., Rivas, M.A., Ruano-Rubio, V., Rose, S.A., Ruderfer, D.M., Shakir, K., Stenson, P.D., Stevens, C., Thomas, B.P., Tiao, G., Tusie-Luna, M.T., Weisburd, B., Won, H.H., Yu, D., Altshuler, D.M., Ardissino, D., Boehnke, M., Danesh, J., Donnelly, S., Elosua, R., Florez, J.C., Gabriel, S.B., Getz, G., Glatt, S.J., Hultman, C.M., Kathiresan, S., Laakso, M., McCarroll, S., McCarthy, M.I., McGovern, D., McPherson, R., Neale, B.M., Palotie, A., Purcell, S.M., Saleheen, D., Scharf, J.M., Sklar, P., Sullivan, P.F., Tuomilehto, J., Tsuang, M.T., Watkins, H.C., Wilson, J.G., Daly, M.J., and MacArthur, D.G., and Exome Aggregation Consortium. (2016). Analysis of protein-coding genetic variation in 60,706 humans. Nature. *536*(7616):285-291.

44- Li, H., and Durbin, R. (2009). Fast and accurate short read alignment with Burrows-Wheeler transform. Bioinformatics *25*, 1754–1760.

45- Lin, Z., Wang, T., Sun, G., and Huang, X. (2010). Report of a case of Zimmermann-Laband syndrome with new manifestations. Int. J. Oral. Maxillofac. Surg. *39*(9):937-941.

46- Lindhurst, M.J., Sapp, J.C., Teer, J.K., Johnston, J.J., Finn, E.M., Peters, K., Turner, J., Cannons, J.L., Bick, D., Blakemore, L., Blumhorst, C., Brockmann, K., Calder, P., Cherman, N., Deardorff, M.A., Everman, D.B., Golas, G., Greenstein, R.M., Kato, B.M., Keppler-Noreuil, K.M., Kuznetsov, S.A., Miyamoto, R.T., Newman, K., Ng, D., O'Brien, K., Rothenberg, S., Schwartzentruber, D.J., Singhal, V., Tirabosco, R., Upton, J., Wientroub, S., Zackai, E.H., Hoag, K., Whitewood-Neal, T., Robey, P.G., Schwartzberg, P.L., Darling, T.N., Tosi, L.L., Mullikin, J.C., and Biesecker, L.G. (2011). A mosaic activating mutation in AKT1 associated with the Proteus syndrome. N. Engl. J. Med. *365*(7):611-619.

47- McKenna, A., Hanna, M., Banks, E., Sivachenko, A., Cibulskis, K., Kernytsky, A., Garimella, K., Altshuler, D., Gabriel, S., Daly, M., and DePristo, M.A. (2010). The Genome Analysis Toolkit: a MapReduce framework for analyzing next-generation DNA sequencing data. Genome Res. *20*(9):1297-1303.

48- Mégarbané, A., Al-Ali, R., Choucair, N., Lek, M., Wang, E., Ladjimi, M., Rose, C.M., Hobeika, R., Macary, Y., Temanni, R., Jithesh, P.V., Chouchane, A., Sastry, K.S., Thomas, R., Tomei, S., Liu, W., Marincola, F.M., MacArthur, D., and Chouchane, L. (2016). Temple-Baraitser Syndrome and Zimmermann-Laband Syndrome: one clinical entity? BMC Med. Genet. *17*(1):42.

49- Mongan, N.P., Jääskeläinen, J., Green, K., Schwabe, J.W., Shimura, N., Dattani, M., and Hughes, I.A. (2002). Two de novo mutations in the AR gene cause the complete androgen insensitivity syndrome in a pair of monozygotic twins. J. Clin. Endocrinol. Metab. *87*(3):1057-1061.

50- Mortensen, L.S., Schmidt, H., Farsi, Z., Barrantes-Freer, A., Rubio, M.E., Ufartes, R., Eilers, J., Sakaba, T., Stühmer, W., and Pardo, L.A. (2015). KV 10.1 opposes activity-dependent increase in Ca2+ influx into the presynaptic terminal of the parallel fibre-Purkinje cell synapse. J. Physiol. *593*(1):181-196.

51- Oliveira Alves, M.G., Carta, C.F., Padín-Iruegas, M.E., Pérez-Sayáns, M., Suarez-Peñaranda, J.M., Issa, J.S., García-García, A., and Almeida, J.D. (2016). Expression of ATP6V1C1 during oral carcinogenesis. Biotech. Histochem. *91*(4):263-268.

52- Ouadid-Ahidouch, H., Ahidouch, A., and Pardo, L.A. (2016). Kv10.1 K(+) channel: from physiology to cancer. Pflugers Arch. *468*(5):751-762.

53- Pardo, L.A., del Camino, D., Sánchez, A., Alves, F., Brüggemann, A., Beckh, S., and Stühmer, W. (1999). Oncogenic potential of EAG K(+) channels. EMBO J. *18*(20):5540-5547.

54- Pfeiffer, R.A., Seemanova, E., Süss, J., Müssig, D., and Tietze, H.U. (1992). The Zimmermann-Laband syndrome. Klin. Padiatr. *204*(1):1-5.

55- Pina-Neto, J. M., Martelli-Soares, L. R., Oliveira-Souza, A. H., Lopes-Petean, E. B., Velludo, M. A. S. L., Campos de Freitas, A., Ribas, J. P. (1988). A new case of Zimmerman-Laband syndrome with mild mental retardation, asymmetry of limbs, and hypertrichosis. (Letter) Am. J. Med. Genet. *31*:691-695.

56- Poëa-Guyon, S., Ammar, M.R., Erard, M., Amar, M., Moreau, A.W., Fossier, P., Gleize, V., Vitale, N., and Morel, N. (2013). The V-ATPase membrane domain is a sensor of granular pH that controls the exocytotic machinery. J. Cell. Biol. *203*(2):283-298.

57- Ramos Gomes, F., Romaniello, V., Sánchez, A., Weber, C., Narayanan, P., Psol, M., and Pardo, L.A. (2015). Alternatively Spliced Isoforms of KV10.1 Potassium Channels Modulate Channel Properties and Can Activate Cyclin-dependent Kinase in Xenopus Oocytes. J. Biol. Chem. *290*(51):30351-30365.

58- Reva, B., Antipin, Y., and Sander, C. (2007). Determinants of protein function revealed by combinatorial entropy optimization. Genome Biol. *8*(11):R232.

59- Reva, B., Antipin, Y., and Sander, C. (2011). Predicting the functional impact of protein mutations: application to cancer genomics. Nucleic Acids Res. *39*(17):e118.

60- Robertson, S. P., Lipp, H., and Bankier, A. (1998). Zimmermann-Laband syndrome in an adult: long-term follow-up of a patient with vascular and cardiac complications. Am. J. Med. Genet. *78*:160-164.

61- Salipante, S.J., Benson, K.F., Luty, J., Hadavi, V., Kariminejad, R., Kariminejad, M.H., Rezaei, N., and Horwitz, M.S. (2007). Double de novo mutations of ELA2 in cyclic and severe congenital neutropenia. Hum. Mutat. *28*(9):874-881.

62- Sánchez, A., Urrego, D., and Pardo, L.A. (2016). Cyclic expression of the voltage-gated potassium channel KV10.1 promotes disassembly of the primary cilium. EMBO Rep. *17*(5):708-723.

63- Sawaki, K., Mishima, K., Sato, A., Goda, Y., Osugi, A., and Nakano, M. (2012). Zimmermann-Laband syndrome: a case report. J. Clin. Pediatr. Dent. *36*(3):297-300.

64- Schuster, A.M., Glassmeier, G., and Bauer, C.K. (2011). Strong activation of ether-à-go-go-related gene 1 K+ channel isoforms by NS1643 in human embryonic kidney 293 and Chinese hamster ovary cells. Mol. Pharmacol. *80*(5):930-942.

65- Schwarz, J.M., Cooper, D.N., Schuelke, M., and Seelow, D. (2014). **MutationTaster2: mutation prediction for the deep-sequencing age.** Nat. Methods. *11*(4):361-362.

66- Shah, N., Gupta, Y. K., and Ghose, S. (2004). Zimmermann-Laband syndrome with bilateral developmental cataract--a new association? Int. J. Paediat. Dent. *14*:78-85.

67- Shihab, H.A., Gough, J., Cooper, D.N., Stenson, P.D., Barker, G.L., Edwards, K.J., Day, I.N., and Gaunt, T.R. (2013). Predicting the functional, molecular, and phenotypic consequences of amino acid substitutions using hidden Markov models. Hum. Mutat. *34*(1):57-65.

68- Siepel, A., and Haussler, D. (2003). Combining phylogenetic and hidden Markov models in biosequence analysis. Proc. 7th Int'l Conf. on Research in Computational Molecular Biology (RECOMB '03), 277-286.

69- Simons, C., Rash, L.D., Crawford, J., Ma, L., Cristofori-Armstrong, B., Miller, D., Ru, K., Baillie, G.J., Alanay, Y., Jacquinet, A., Debray, F.G., Verloes, A., Shen, J., Yesil, G., Guler, S., Yuksel, A., Cleary, J.G., Grimmond, S.M., McGaughran, J., King, G.F., Gabbett, M.T., and Taft, R.J. (2015). Mutations in the voltage-gated potassium channel gene KCNH1 cause Temple-Baraitser syndrome and epilepsy. Nat. Genet. *47*(1):73-77.

70- Stefanova, M., Atanassov, D., Krastev, T., Fuchs, S., Kutsche, K. (2003). Zimmermann-Laband syndrome associated with a balanced reciprocal translocation t(3;8)(p21.2;q24.3) in mother and daughter: molecular cytogenetic characterization of the breakpoint regions. Am. J. Med. Genet. *117A*:289-294.

71- Steinberg, B.E., Huynh, K.K., Brodovitch, A., Jabs, S., Stauber, T., Jentsch, T.J., and Grinstein, S. (2010). A cation counterflux supports lysosomal acidification. J. Cell. Biol. *189*(7):1171-1186.

72- Stengel, R., Rivera-Milla, E., Sahoo, N., Ebert, C., Bollig, F., Heinemann, S.H., Schönherr, R., and Englert, C. (2012). Kcnh1 voltage-gated potassium channels are essential for early zebrafish development. J. Biol. Chem. *287*(42):35565-35575.

73- Sun-Wada, G.H., and Wada, Y. (2015). Role of vacuolar-type proton ATPase in signal transduction. Biochim. Biophys. Acta. *1847*(10):1166-1172.

74- Temple, I. K., and Baraitser, M. (1991). Severe mental retardation and absent nails of hallux and pollex. Am. J. Med. Genet. *41*:173-175.

75- Tessitore, A., Sinisi, A.A., Pasquali, D., Cardone, M., Vitale, D., Bellastella, A., and Colantuoni, V. (1999). A novel case of multiple endocrine neoplasia type 2A associated with two de novo mutations of the RET protooncogene. J. Clin. Endocrinol. Metab. *84*(10):3522-3527.

76- Ufartes, R., Schneider, T., Mortensen, L.S., de Juan Romero, C., Hentrich, K., Knoetgen, H., Beilinson, V., Moebius, W., Tarabykin, V., Alves, F., Pardo, L.A., Rawlins, J.N., and

Stuehmer, W. (2013). Behavioural and functional characterization of Kv10.1 (Eag1) knockout mice. Hum. Mol. Genet. *22*(11):2247-2262.

77- Urrego, D., Movsisyan, N., Ufartes, R., and Pardo, L.A. (2016). Periodic expression of Kv10.1 driven by pRb/E2F1 contributes to G2/M progression of cancer and non-transformed cells. Cell Cycle. *15*(6):799-811.

78- van Bon, B.W., Gilissen, C., Grange, D.K., Hennekam, R.C., Kayserili, H., Engels, H., Reutter, H., Ostergaard, J.R., Morava, E., Tsiakas, K., Isidor, B., Le Merrer, M., Eser, M., Wieskamp, N., de Vries, P., Steehouwer, M., Veltman, J.A., Robertson, S.P., Brunner, H.G., de Vries, B.B., and Hoischen, A. (2012). Cantú syndrome is caused by mutations in ABCC9. Am. J. Hum. Genet. *90*(6):1094-1101.

79- Van Buggenhout, G. J. C. M., Brunner, H. G., Trommelen, J. C. M., and Hamel, B. C. J. (1995). Zimmermann-Laband syndrome in a patient with severe mental retardation. Genet. Counsel. *6*:321-327.

80- Vitavska, O., Wieczorek, H., and Merzendorfer, H. (2003). A novel role for subunit C in mediating binding of the H+-V-ATPase to the actin cytoskeleton. J. Biol. Chem. *278*(20):18499-18505.

81- Vitavska, O., Merzendorfer, H., and Wieczorek, H. (2005). The V-ATPase subunit C binds to polymeric F-actin as well as to monomeric G-actin and induces cross-linking of actin filaments. J. Biol. Chem. *280*(2):1070-1076.

82- Yuan, Y., Zhang, J., Chang, Q., Zeng, J., Xin, F., Wang, J., Zhu, Q., Wu, J., Lu, J., Guo, W., Yan, X., Jiang, H., Zhou, B., Li, Q., Gao, X., Yuan, H., Yang, S., Han, D., Mao, Z., Chen, P., Lin, X., and Dai, P. (2014). *De novo* mutation in ATP6V1B2 impairs lysosome acidification and causes dominant deafness-onychodystrophy syndrome. Cell Res. *24*(11):1370-1373.

83- Zhang, Y.Y., Yue, J., Che, H., Sun, H.Y., Tse, H.F., and Li, G.R. (2014). BKCa and hEag1 channels regulate cell proliferation and differentiation in human bone marrow-derived mesenchymal stem cells. J. Cell Physiol. *229*(2):202-212.

84- Zimmermann, K. W. (1928). Ueber Anomalien des Ektoderms. Vjschr. Zahnheilk. *44*:419-434.

8. Publications and posters

Kortüm, F., Caputo, V., Bauer, C.K., Stella, L., Ciolfi, A., Alawi, M., Bocchinfuso, G., Flex, E., **Paolacci, S.**, Dentici, M.L., Grammatico, P., Korenke, G.C., Leuzzi, V., Mowat, D., Nair, L.D., Nguyen, T.T., Thierry, P., White, S.M., Dallapiccola, B., Pizzuti, A., Campeau, P.M., Tartaglia, M., and Kutsche, K. (2015). Mutations in KCNH1 and ATP6V1B2 cause Zimmermann-Laband syndrome. Nat. Genet. *47*(6):661-667.

Flex, E., Jaiswal, M., Pantaleoni, F., Martinelli, S., Strullu, M., Fansa, E.K., Caye, A., De Luca, A., Lepri, F., Dvorsky, R., Pannone, L., **Paolacci, S.**, Zhang, S.C., Fodale, V., Bocchinfuso, G., Rossi, C., Burkitt-Wright, E.M., Farrotti, A., Stellacci, E., Cecchetti, S., Ferese, R., Bottero, L., Castro, S., Fenneteau, O., Brethon, B., Sanchez, M., Roberts, A.E., Yntema, H.G., Van Der Burgt, I., Cianci, P., Bondeson, M.L., Cristina Digilio, M., Zampino, G., Kerr, B., Aoki, Y., Loh, M.L., Palleschi, A., Di Schiavi, E., Carè, A., Selicorni, A., Dallapiccola, B., Cirstea, I.C., Stella, L., Zenker, M., Gelb, B.D., Cavé, H., Ahmadian, M.R., and Tartaglia, M. (2014). Activating mutations in RRAS underlie a phenotype within the RASopathy spectrum and contribute to leukaemogenesis. Hum. Mol. Genet. *23*(16):4315-4327.

Caputo, V., Chong, J.X., Phelps, I.G., Stella, L., Worgan, L., Dempsey, J.C., Nguyen, A., **Paolacci, S.**, Leuzzi, V., Webster, R., Pizzuti, A., Marvin, C.T., Ishak, G.E., Ardern–Holmes, S., Richmond, Z., Bamshad, M.J., Ortiz-Gonzalez, X.R., Chopra, M., Doherty, D., and Tartaglia, M. (2016). Recessive inactivating mutations in TBCK, a Rab GTPase-activating protein that modulates mTOR signaling, cause severe infantile syndromic encephalopathy. In: The European Human Genetics Conference 2016, Barcelona, Spain, May 21-24.

Paolacci, S., Caputo, V., Bruselles, A., Ciolfi, A., Giovannetti, A., Bertini, E., Pizzuti, A., Leuzzi, V., and Tartaglia, M. (2015). Novel POLR3A mutations causing hypomyelinating leukodystrophy. In: XVIII Congresso Nazionale SIGU. Rimini, Italy, October 21-24.

Kortüm F, Caputo V, Bauer CK, Stella L, Ciolfi A, Alawi M, Bocchinfuso G, Flex E, **Paolacci S.**, Dentici ML, Grammatico P, Korenke GC, Leuzzi V, Mowat D, Nair LDV, Nguyen TTM, Thierry P, White SM, Dallapiccola B, Pizzuti A, Campeau PM, Tartaglia M, Kutsche K (2015). Mutations in KCNH1 and ATP6V1B2 cause Zimmermann-Laband syndrome. In: The European Human Genetics Conference 2015. Glasgow, Scotland, United Kingdom, June 6-9.